BRAIN
A JOURNAL OF NEUROLOGY

Brain cancer induces systemic immunosuppression through release of non-steroid soluble mediators

Katayoun Ayasoufi,[1] Christian K. Pfaller,[2,3] Laura Evgin,[2] Roman H. Khadka,[1,4] Zachariah P. Tritz,[1,4] Emma N. Goddery,[1,4] Cori E. Fain,[1,4] Lila T. Yokanovich,[1,4] Benjamin T. Himes,[1,5] Fang Jin,[1] Jiaying Zheng,[2,4] Matthew R. Schuelke,[1,2,4,6] Michael J. Hansen,[1] Wesley Tung,[1] Ian F. Parney,[1,5] Larry R. Pease,[1] Richard G. Vile[1,2] and Aaron J. Johnson[1,2,7]

Immunosuppression of unknown aetiology is a hallmark feature of glioblastoma and is characterized by decreased CD4 T-cell counts and downregulation of major histocompatibility complex class II expression on peripheral blood monocytes in patients. This immunosuppression is a critical barrier to the successful development of immunotherapies for glioblastoma. We recapitulated the immunosuppression observed in glioblastoma patients in the C57BL/6 mouse and investigated the aetiology of low CD4 T-cell counts. We determined that thymic involution was a hallmark feature of immunosuppression in three distinct models of brain cancer, including mice harbouring GL261 glioma, B16 melanoma, and in a spontaneous model of diffuse intrinsic pontine glioma. In addition to thymic involution, we determined that tumour growth in the brain induced significant splenic involution, reductions in peripheral T cells, reduced MHC II expression on blood leucocytes, and a modest increase in bone marrow resident CD4 T cells. Using parabiosis we report that thymic involution, declines in peripheral T-cell counts, and reduced major histocompatibility complex class II expression levels were mediated through circulating blood-derived factors. Conversely, T-cell sequestration in the bone marrow was not governed through circulating factors. Serum isolated from glioma-bearing mice potently inhibited proliferation and functions of T cells both in vitro and in vivo. Interestingly, the factor responsible for immunosuppression in serum is non-steroidal and of high molecular weight. Through further analysis of neurological disease models, we determined that the immunosuppression was not unique to cancer itself, but rather occurs in response to brain injury. Non-cancerous acute neurological insults also induced significant thymic involution and rendered serum immunosuppressive. Both thymic involution and serum-derived immunosuppression were reversible upon clearance of brain insults. These findings demonstrate that brain cancers cause multifaceted immunosuppression and pinpoint circulating factors as a target of intervention to restore immunity.

1 Mayo Clinic Department of Immunology, Rochester, MN, USA
2 Mayo Clinic Department of Molecular Medicine, Rochester, MN, USA
3 Paul-Ehrlich-Institute, Division of Veterinary Medicine, Langen, Germany
4 Mayo Clinic Graduate School of Biomedical Sciences, Rochester, MN, USA
5 Mayo Clinic Department of Neurologic Surgery, Rochester, MN, USA
6 Department of Immunology, Mayo Clinic Medical Scientist Training Program, Rochester, Minnesota, USA
7 Mayo Clinic Department of Neurology, Rochester, MN, USA

Correspondence to: Aaron J. Johnson, PhD
Professor and Consultant, Departments of Immunology, Neurology, and Molecular Medicine,
Guggenheim 4-11C, Mayo Clinic, 200 First St. SW, Rochester, MN 55905, USA
E-mail: Johnson.aaron2@mayo.edu

Introduction

Glioblastoma (GBM) is an incurable malignant brain tumour with poor prognosis that affects over 12 000 patients annually in the USA alone (Ostrom *et al.*, 2015). Systemic immunosuppression is a hallmark feature of GBM and other neurological insults including stroke, and traumatic brain injury (Dix *et al.*, 1999; Meisel *et al.*, 2005; Fecci *et al.*, 2006; Vega *et al.*, 2008; Gustafson *et al.*, 2010; Grossman *et al.*, 2011; Chongsathidkiet *et al.*, 2018; Ritzel *et al.*, 2018). This immunosuppression, especially in GBM, is a critical barrier to both patient survival and efficacy of immune-modulating therapies. GBM patients can have CD4 T-cell counts comparable to those with acquired immunodeficiency syndrome (AIDS), yet current efforts are focused on developing and improving immunomodulatory therapies that will be ineffective in immunosuppressed individuals (Gustafson *et al.*, 2010; Chongsathidkiet *et al.*, 2018). While the presence of immunosuppression in neurological diseases has become an accepted feature of these conditions, the exact immunological nature and the underlying mechanisms of this immunosuppression remain largely unknown.

A major focus of neuroimmunology research has been the activation, infiltration and induction of neuropathology by immune cells (Lewicki *et al.*, 2003; Johnson *et al.*, 2005; McDole *et al.*, 2006; Ferretti *et al.*, 2016; Willenbring *et al.*, 2016; Huggins *et al.*, 2017; Huseby Kelcher *et al.*, 2017; Laurent *et al.*, 2017; Malo *et al.*, 2018*a*, *b*; Ransehoff, 2018). However, neuro-immune interactions are bidirectional, as recently highlighted by studies demonstrating that the nervous system affects functions of the immune system, including bacterial clearance, ageing, allergy, and itch responses through neuronal connections and/or release of soluble factors at the site of injury (Wong, 2011; Talbot *et al.*, 2015; Stanley *et al.*, 2016; Liu *et al.*, 2017; Voisin *et al.*, 2017; Baral *et al.*, 2018; Kipnis and Filiano, 2018; Maryanovich *et al.*, 2018; Pinho-Ribeiro *et al.*, 2018). These studies have immensely enhanced our understanding of communication between the peripheral nervous system and the immune system under several conditions. However, it remains unclear how neurological diseases, especially GBM, lead to immunosuppression not only within the brain/tumour microenvironment, but also outside of the brain.

Peripheral immunosuppression during neurological insults affects both primary and secondary immune organs (Meisel *et al.*, 2005; Hazeldine *et al.*, 2015; Liu *et al.*, 2017). All organs are innervated (Kendall and Al-Shawaf, 1991; Antonica *et al.*, 1994; Mignini *et al.*, 2003). While the function of organ innervation is well-established for endocrine, circulatory and pulmonary systems, the function of

innervation in primary and secondary immune organs is less well defined. Studies linking injury in the brain to a direct and measurable change in the immune system will help determine the mechanisms through which neurological diseases cause severe immunosuppression, and evaluate whether that immunosuppression is mediated through innervation and/or release of soluble factors.

The thymus is the critical primary immune organ responsible for generating and educating T cells. Additionally, the thymus is crucial in maintaining peripheral T-cell counts in both children and adults (Zhang *et al.*, 1999; van den Broek *et al.*, 2016). As T-cell development and education exclusively require a functional thymus, changes in thymic homeostasis have long lasting immunological consequences (Williams *et al.*, 2007; van den Broek *et al.*, 2016). Once believed to be less important in maintaining a healthy immune system in adults, numerous studies have highlighted the crucial role of the adult thymus in generating peripheral T cells under conditions of lymphopaenia (Jamieson *et al.*, 1999; Roux *et al.*, 2000; Williams *et al.*, 2007; Ferrando-Martínez *et al.*, 2009; van den Broek *et al.*, 2016; Ayasoufi *et al.*, 2017; Rosado-Sanchez *et al.*, 2017). Patients devoid of a functional thymus cannot reconstitute their T cell repertoire following haematopoietic transplantation, HIV infection, chemotherapy, and general immunosuppression (Jamieson *et al.*, 1999; Zhang *et al.*, 1999; Roux *et al.*, 2000; Williams *et al.*, 2007; Ferrando-Martínez *et al.*, 2009; van den Broek *et al.*, 2016; Rosado-Sanchez *et al.*, 2017). Importantly, the adult thymus is still generating new T cells into the seventh decade of life (Jamieson *et al.*, 1999; Williams *et al.*, 2007). For these reasons, we aimed to study the role of brain-thymus communication during immunosuppression induced by GBM and other neurological insults. We hypothesized that systemic immunosuppression following neurological insults is exacerbated due to direct detrimental effects of brain injury on thymic homeostasis.

In this study, we investigated the extent to which the thymus responds to insults, including experimental GBM, which are contained within the CNS. In addition, we go beyond the thymus and evaluate the changes within spleen, peripheral blood, serum, and bone marrow of glioma-bearing mice. We report that the brain-thymus axis is one significant part of a multifaceted systemic immunosuppression during glioma progression and following other neurological insults. Our studies further demonstrate that the mechanisms leading to this immunosuppression involve release of non-steroid soluble factors following brain injury. These results help us better understand changes in the immune system following brain insults, and provide new insights into mechanisms of immunosuppression induced by brain cancers.

Materials and methods

Mice

Male and female (wild-type) C57BL/6, (GFP) C57BL/6-Tg (UBC-GFP) 30Scha/J, and MHCII$^{-/-}$ (B6-12952-$^{H2d1Ab1-EA}$/J) mice were purchased from Jackson Laboratory (Cat. #000664, #004353, and #003584, respectively). GFP mice express GFP under the Ubiquitin-C promoter which is expressed in all tissues. GFP and MHCII$^{-/-}$ mice were bred in our facility. Adrenalectomized mice were purchased from Jackson Laboratory and maintained on 1% saline in drinking water for the duration of experiments. Mice were bred and maintained at Mayo Clinic under Institutional Animal Care and Use Committee (IACUC) guidelines. Handling of all animals and performing of all procedures were approved by Mayo Clinic IACUC.

Intracranial injection

Mice were anaesthetized by intraperitoneal injection of 30 mg/kg ketamine and 3 mg/kg xylazine. Under anaesthesia, a 0.5-cm longitudinal incision was made on the scalp and a right frontal burr hole was drilled into ~1-mm lateral and 2-mm anterior to bregma as previously described (Malo et al., 2018a, b). Using a stereotactic frame, the needle of a Hamilton syringe (Hamilton Company) was lowered 3.3 mm into the cortex and retracted 0.3 mm. At this depth, injections were performed in a total volume of 1.5–2 μl. We injected half of the volume followed by a 2-min pause. The second half of the volume was injected followed by a 3-min pause before the needle was retracted. The wound was closed using 4-0 vicryl suture (Ethicon Inc). This method was used for injection of phosphate-buffered saline (PBS), lipopolysaccharide (LPS), GL261 cells, and B16-F1 melanoma cells.

TMEV infection

For intracranial Theiler's murine encephalomyelitis virus (TMEV) infections, mice were anaesthetized with 2% isoflurane and given an intracerebral injection with 2×10^6 PFU of Daniel's strain of TMEV in a 10 μl volume as previously published (Johnson et al., 2005). For intraperitoneal infection, mice were given an intraperitoneal injection with 2×10^7 PFU of Daniel's strain of TMEV in a 100 μl volume. TMEV was made by Dr Kevin Pavelko at Mayo Clinic (Rochester, MN) (Pavelko et al., 2011; Bell et al., 2014).

Vesicular stomatitis virus encoding ovalbumin infection and tetramer staining

Vesicular stomatitis virus encoding ovalbumin (VSV-OVA) was kindly prepared and provided by the laboratory of Dr Richard Vile as previously reported (Wongthida et al., 2011). Mice were infected with 10^7 PFU intravenously. Antigen-specific responses were quantified using K^b:OVA (SIINFEKL) tetramers. Tetramers were provided by the NIH tetramer facility (Atlanta, GA).

Tumour cell culture

GL261-Luciferase (GL261-Luc) expressing cells were provided by the laboratory of Dr John Ohlfest (Masonic Cancer Center University of Minnesota, Minneapolis, MN). GL261-Luc cells were grown in Dulbecco's modified Eagle medium (DMEM, Gibco) with L-glutamine supplemented with 10% foetal bovine serum (FBS) and 1% penicillin/streptomycin (Sigma). We used trypsin L express (Cat. #12605-010 Gibco) to detach confluent cells. We injected 60 000 GL261-Luc cells or 10 000 B16-F1 melanoma cells (provided by Dr Vile's laboratory) according to an intracranial injection procedure.

Spontaneous murine glioma model

The replication-competent avian sarcoma-leukosis virus with splice-acceptor (RCAS)-based spontaneous murine glioma system was a generous gift of Dr Oren Becher (Northwestern University) and was used as previously described (Cordero et al., 2017).

Bioluminescence imaging

The tumour burden in GL261-Luc-bearing mice was assessed using bioluminescence imaging as previously described (Malo et al., 2018b). Mice were intraperitoneally injected with 150 mg/kg D-luciferin sodium salt in PBS (Gold Biotechnology) and anaesthetized with 2.5% isoflurane before imaging. 0.5–1% isoflurane was used to maintain anaesthesia during imaging. Mice were scanned using Mayo Clinic's IVIS Spectrum system (Xenogen Corp.) running Living Image software.

Seizure induction

A saline kainic acid (KA) solution was prepared at 2 mg/ml. Mice received 15.5–17.5 mg/kg of KA solution through an intraperitoneal injection. To stop seizure activity at 90 min post KA injection, all mice received valproic acid (Sigma) at 300 mg/kg concentration from a solution of 45 mg/ml made in saline. We used a modified Racine score to measure seizure activity as previously described (Racine, 1972; Eyo et al., 2014).

Organ processing

Spleens and thymi were dissected and weighed before dissociation using the rubber end of a syringe in RPMI 1640 (Gibco). To evaluate thymic epithelial cells, we enzymatically digested the thymi according to the manufacturer's guidelines using gentleMACS^{TM} Octo Dissociator and tumour dissociation enzymatic digestion kit (Miltenyi Biotec, Cat. #130-096-730). For bone marrow isolation, PBS was injected using a 21G needle to flush cells. Red blood cells were lysed using ammonium-chloride-potassium (ACK) lysis buffer (8.3 g NH$_4$Cl, 1 g KCl, 250 μl of 0.5 M EDTA made up to 1 l with water pH 7.2–7.4). Brains were mechanically homogenized using the Dounce method followed by 38% Percoll (Sigma) centrifugation as previously published (Cumba Garcia et al., 2016). Blood was collected from the tail vein and immediately placed in heparin working solution. A 1000-unit heparin solution (Sigma) was made in water. This solution was diluted 1:4 with PBS to generate a heparin working solution. Following ACK lysis and washing steps, pellets were prepared. Cells were then counted using a

haemocytometer (Hausser Scientific) with trypan blue exclusion (Gibco). Cells were stained with appropriate antibodies for 30 min at 4°C and washed twice with PBS (Corning) and analysed using flow cytometry.

Antibodies and flow cytometry

FITC anti-CD8 (BD Pharmingen, Cat. #553031), FITC anti-MHCII (BioLegend, Cat. #107605), PE anti-CD44 (BD Pharmingen, Cat. #553134), APC anti-CD4 (BioLegend, Cat. #100515), PE-Cy7 anti-CD8a (BD, Cat. #552877), PE-Cy7 anti-TCRβ (eBioscience, Cat. #60-5961), Percp anti-CD45 (BioLegend, Cat. #103130), BV785 anti-CD8 (BioLegend, Cat. #100750), BV786 anti-CD4 (BD Horizon, Cat. #563727), Pacific Blue anti-IA/IE (BioLegend, Cat. #107620), BV421 anti-CD25 (BioLegend, Cat. #102033), PE-Cy7 anti-Epcam (BioLegend, Cat. #118215), and BV711 anti-CD45 (BioLegend, Cat. #103147) antibodies were used at 1:100 dilution to stain cells isolated from all organs, and at 1:1000 dilution to stain blood cells. Ghost red-780 viability dye (Tonbo, Cat. #13-0865-T100) was used at a 1:1000 concentration to stain dead cells. Cells were analysed using an LSRII flow cytometer (BD). Experiments presented in Supplementary Fig. 1F–H were analysed on a Cytek Aurora flow cytometer. Data were analysed on FlowJo 10.1 (FlowJo LLC, Ashland, OR).

CFSE labelling and *in vitro* T-cell proliferation assay

Isolated cells from spleens and lymph nodes of naïve unmanipulated C57BL/6 mice were placed in RoboSep^{TM} buffer (Stemcell Technologies) at 5×10^7 cells/ml. CFSE (1 µl/ml) [BioLegend, 5 mM in dimethyl sulphoxide (DMSO) stock] was added at a final concentration of 5 µM followed by a 10-min incubation at room temperature. Following washes with complete-RPMI, cells were resuspended at 10^8 cells/ml in RoboSep^{TM} buffer. T-cell isolation was performed using EasySep^{TM} mouse negative T-cell isolation kit (Stemcell Technologies, Cat. #19851) according to the manufacturer's instructions. To plated cells, anti-CD3/CD28 beads (Dynabeads, Gibco, Cat. #11452D) were added at a 3:1 ratio of beads to cells. After 72 h, T cells were separated from beads using a magnet (Stemcell Technologies) and CFSE dilution was analysed by flow cytometry.

Molecular weight analysis of serum

Sera were diluted in PBS and passed through a 3 kDa filter (Pierce ThermoScentific, Cat. #88512) according to the manufacturer's instructions. Top fragment (>3 kDa) was then sequentially passed through 10 kDa, 30 kDa, and 100 kDa (Pierce ThermoScientific, Cat. #88513, #88502, #88503) filters. Immunosuppressive capacities of all generated fractions were tested.

RNA extraction, quality control and DNase treatment

Thymi were flash frozen in liquid nitrogen upon extraction from the mouse and stored at –80°C. Frozen thymi were placed in TRIzol® (Ambion, Life Technologies) and homogenized using an electric homogenizer (Fisherbrand 150 homogenizer), followed by RNA isolation as previously described (Pfaller *et al.*, 2018). RNA quality was assessed by agarose gel electrophoresis and capillary transfer onto nylon membranes, followed by methylene blue staining. For library preparation, 3 µg of total RNA were treated with DNaseI (Invitrogen, Cat. #18068-015) and impurities were eliminated using RNeasy® columns (Qiagen, RNeasy Mini kit Cat. #74104) according to the manufacturer's instructions.

Library preparation and RNA sequencing using Illumina TruSeq v2 mRNA protocol

RNA libraries were prepared using 100 ng of total RNA according to the manufacturer's instructions for the TruSeq RNA Sample Prep Kit v2 (Illumina) employing poly-A mRNA enrichment using oligo-dT magnetic beads. The final adapter-modified cDNA fragments were enriched by 12 cycles of PCR using Illumina TruSeq PCR primers. The concentration and size distribution of the completed libraries was determined using a Fragment Analyzer (AATI) and Qubit fluorometry (Invitrogen). Libraries were sequenced at 30–40 million fragment reads per sample following Illumina's standard protocol using the Illumina-cBot and HiSeq-3000/4000-PE Cluster Kit. The flow cells were sequenced as 100×2 paired end reads on an Illumina HiSeq-4000 using HiSeq-3000/4000 sequencing kit and HD3.4.0.38 collection software. Base-calling was performed using Illumina's RTA version 2.7.7.

RNA sequencing analysis

We used tools available on the Galaxy platform (https://usegalaxy.org). The paired-end reads were aligned to the mouse reference genome mm10 (GRCm38.p6; GenBank accession number GCA_000001635.8) using HISAT2 and exon read count tables were generated using DEXSeq-Count (v.1.24.0.0). Counts were normalized per million total reads and Log2-transformed. A two-dimensional principal component analysis (PCA) was then performed using Microsoft Excel. Significant changes in the gene expression patterns were assessed by one-way ANOVA followed by a two-tailed Student's *t*-test. Pathway enrichment was calculated for genes that were significantly up- or downregulated at least 2-fold using Panther GO-slim pathway analysis (www.pantherdb.org) and ingenuity pathway analysis (www.ingenuity.com).

Parabiosis

Two female mice of similar weight and age were co-housed for 2 weeks prior to surgery to ensure harmonious cohabitation. Our parabiosis procedure protocol was adapted from Kamran, *et al.* (2013) and modified according to the IACUC at Mayo Clinic. Anaesthesia was induced and maintained with ketamine/xylazine as before. For analgesia, we administered carprofen and buprenorphine-SR subcutaneously at a dose of 5 mg/kg and 1 mg/kg, respectively. We treated mice with enrofloxacin (50 mg/kg) in drinking water for 10 days to prevent bacterial infections.

Statistical analysis and graphics

GraphPad prism 8.0.1 (La Jolla, CA) was used for figure generation and statistical analysis. Either Mann-Whitney U rank sum test or a one-way ANOVA with *post hoc* analysis or χ^2 survival analysis was used to assess statistical significance. The specific tests used are detailed in figure legends. All data are represented as individual data-points with mean ± standard deviation (SD). Biorender.com was used to create the graphical abstract and some schematics.

Data availability

All data will be made available upon request. Please contact the corresponding author.

Results

Experimental models of brain cancer induce sustained thymic involution

Brain cancers are associated with severe immunosuppression (Meisel *et al.*, 2005; Gustafson *et al.*, 2010; Chongsathidkiet *et al.*, 2018). We sought to determine if immunosuppression during brain cancer affects the thymus. To test this, we used the GL261 murine glioma model (Fig. 1A). As a second model of brain cancer, we used intracranial inoculation of B16 melanoma cells (Fig. 1A). We investigated the effect of brain injury due to brain cancers on the thymus at the time mice became moribund. GL261-Luc glioma inoculation is incurable, and all tumour-bearing mice succumb to death (Fig. 1B, survival of tumour-bearing mice is shown). Tumour incidence with GL261-Luc gliomas is between 70% and 90% in our hands. This may be due to the immunogenicity of luciferase protein. As a result, 10–30% of inoculated mice do not develop tumours and serve as tumour-negative controls [tumour (–)]. The thymi of late stage GL261-tumour-bearing mice appeared significantly smaller compared to time-matched/age-matched controls (Fig. 1A). In a larger cohort, we determined that thymic size as measured by weight and cellularity was significantly reduced in GL261 tumour-bearing mice when compared to tumour (–) controls (Fig. 1C and D). Similarly, GL261 implanted mice had smaller thymic weights and cellularities when compared to naïve unmanipulated mice (Fig. 1E and F). Subcutaneous implantation of GL261 cells did not induce thymic involution suggesting that, unlike brain tumours, peripheral cancers may not disrupt thymic homeostasis in a similar manner (Fig. 1G). Next, we sought to determine whether the extent of thymic involution was dependent on the magnitude of brain injury. We took advantage of the heterogeneity in glioma growth in our experiments as mice bearing luciferase-expressing GL261 tumours have varying tumour burdens at the onset of morbidity. This variation in tumour size can be measured using bioluminescence imaging. All animals were moribund at the time of analysis. Mice were sorted based on the intensity of the bioluminescence signal and thymic cellularity was correlated with tumour burden. We found an inverse correlation between thymic cellularity and tumour burden (Fig. 1H). We next sought to evaluate whether our findings were glioma-specific. Similar to GL261 gliomas, implantation of B16 melanoma in the brain induced significant thymic involution compared to sham-injected mice as evident by reductions in both thymic weight and cellularity (Fig. 1I and J). The thymus was not the only immune organ affected by brain tumours. We also found that spleens of GL261 tumour-bearing mice were reduced in size and cellularity compared to controls (Fig. 1K and L). Finally, we tested the extent of thymic involution in the RCAS-based spontaneous murine glioma model of diffuse intrinsic pontine glioma (DIPG) (Fig. 1M). Thymic involution was observed in mice that spontaneously developed gliomas in the brain stem compared to those that did not (Fig. 1N and O). Taken together, our results demonstrate that three distinct experimental brain cancers, which grow in different brain regions, cause similar thymic involution. These data also show that GL261-glioma size correlates with the degree of thymic involution.

Brain tumours dysregulate T-cell development processes in the thymus

Given that glioma growth in the brain induced severe thymic involution, we next sought to determine cellular changes within the affected thymi. We first compared age-matched tumour (–) and naïve thymi and did not find any differences between these groups in our experiments (data not shown). Therefore, both tumour (–) and naïve mice were used as controls interchangeably. To analyse T-cell development within the thymus, we gated on live, CD45$^+$ leucocytes and used CD4 and CD8 markers to determine double-positive (DP) (CD4$^+$CD8$^+$), single-positive (SP)-CD4, (CD4$^+$CD8$^-$), SP-CD8 (CD4$^-$CD8$^+$), and double-negative (DN) (CD4$^-$CD8$^-$) populations (Fig. 2A). Once double-negative populations were identified, we used CD44 and CD25 markers (within the cells in the double-negative gate) to distinguish DN1 (CD44$^+$CD25$^-$), DN2 (CD44$^+$CD25$^+$), DN3 (CD44$^-$CD25$^+$), and DN4 (CD44$^-$CD25$^-$) populations of developing thymocytes (Fig. 2B). Using these gating strategies, we assessed the stage at which T-cell development is affected by a growing glioma in the brain. Frequencies of DN1 cells were significantly increased in GL261 tumour-bearing mice compared to controls (Fig. 2C). Interestingly, this increase in frequencies of DN1 cells translated into normalization of absolute numbers between control and atrophied thymi (Fig. 2C). An increase in frequencies of DN2 cells did not reach statistical significance (Fig. 2D). Similar to DN1 cells, we observed analogous numbers of DN2 cells in both control and atrophied thymi (Fig. 2D). Interestingly, both frequencies and absolute counts of DN3 cells were significantly reduced in tumour-bearing mice compared to
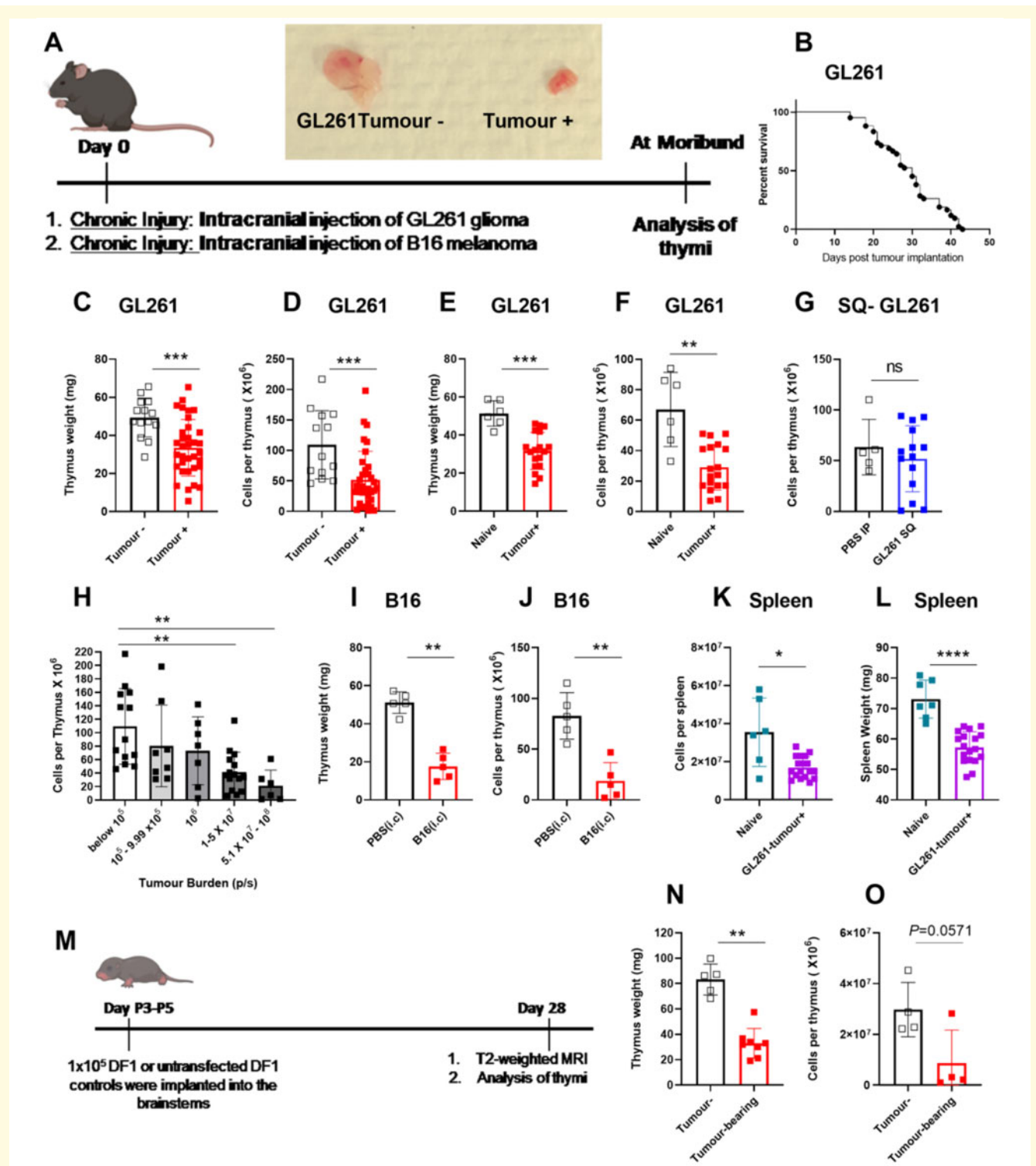
Figure 1 Experimental models of brain cancer induce sustained thymic involution. (**A**) Experimental design is shown. Mice are implanted with 60 000 luciferase-bearing GL261 cells or 10 000 B16-F1 melanoma cells in the frontal lobe of the brain 3-mm deep. Gross analysis of thymi taken from a GL261 tumour- bearing mouse compared to a tumour-negative mouse. Thymi were analysed at the time glioma-bearing mice become moribund. (**B**) Survival of GL261 tumour-bearing mice is shown. Tumour take is 70–90% rendering the remaining 10–30% tumour-negative. Survival plot only shows tumour-bearing mice. (**C**) Thymic weight (**D**) and cellularity is compared between GL261 tumour-bearing and tumour-negative mice at the time glioma-bearing mice become moribund. Tumour-negative and tumour-bearing mice are age-matched. Similarly (**E** and **F**) GL261- bearing mice have significantly smaller thymi as measured by thymic weight and cellularity compared to naïve unmanipulated mice. (**G**) Subcutaneous implantation of GL261-Luc cells did not result in thymic involution. (**H**) Thymic cellularity was inversely correlated with tumour burden in GL261-Luc tumour-bearing mice. Mice were binned based on bioluminescence imaging at the time of euthanasia and thymic cellularity was plotted against tumour burden (as measured by bioluminescence intensity). Bioluminescence intensity (photon/s) was calculated

(continued)

controls (Fig. 2E). This reduction in DN3 cells translated into a significant reduction in frequencies and numbers of DN4 and double-positive cells (Fig. 2F and G). Frequencies of SP-CD4 T cells were significantly increased in glioma-bearing thymi compared to controls (Fig. 2H). This significant increase in frequencies of SP-CD4 T cells led to equalization of absolute numbers between control and atrophied thymi (Fig. 2H). Frequencies of SP-CD8 T cells were also increased in glioma-bearing mice compared to controls (Fig. 2I). However, this increase in frequencies of SP-CD8 T cells was not sufficient to compensate for the loss of cells and hence absolute numbers of thymic SP-CD8 T cells in glioma-bearing mice remained reduced when compared to controls (Fig. 2I).

B-cell developmental programming is normally inhibited in the thymus to maximize generation of functional T cells (Garcia-Ojeda et al., 2013; Scripture-Adams et al., 2014; Rothenberg, 2019). Hence, we evaluated frequencies and numbers of thymic B cells and single-positive T cells that have successfully rearranged their T-cell receptor using flow cytometry (Fig. 2J). Interestingly, we found a significant increase in frequencies of B cells and TCRβ$^+$ T cells in the atrophied thymi obtained from glioma-bearing mice compared to controls (Fig. 2K and L). This significant increase in frequencies of B cells and TCRβ$^+$ T cells resulted in normalization of absolute counts of these populations between control and atrophied thymi (Fig. 2K and L). Thus, our data indicate that experimental GBM induces thymic involution that is associated with dysregulation of T-cell development with simultaneous enhancement of B-cell development.

Brain cancer induces unique transcriptional programs in the thymus

We observed thymic involution in GL261 glioma-bearing mice that was associated with reductions in DN3 thymocytes, retention of single-positive T cells, and enhancement of B-cell development at the cellular level. We next asked whether thymic involution in glioma-bearing mice was associated with distinct transcriptional programs. We used next generation RNA sequencing (RNA-seq) as an unbiased method of analysis that can identify upstream pathways and/or molecules that regulate thymic involution using gene ontology (GO) and ingenuity pathway analysis (IPA) comparing the transcriptomes of thymi of GL261 glioma-bearing mice with sham control (PBS-injected) and naïve unmanipulated mice (Fig. 3A). Thymic RNA was isolated at the time tumour-bearing mice became moribund, and sham and naïve control mice were time- and age-matched. We assessed RNA quality by integrity of ribosomal RNA subunits and selected three GL261 tumour-bearing, PBS sham, and naïve thymi each for RNA-seq (Supplementary Fig. 1A). PCA indicated that transcriptomic profiles of thymi of glioma-bearing mice were distinct from controls (Fig. 3B). Notably, thymic transcriptomes of PBS-injected animals were similar to naïve animals at the time of RNA isolation (between Days 25 and 42 post intracranial injection; Fig. 3B). We found a significantly altered gene expression pattern in thymi from GL261-bearing mice compared to naïve mice (Fig. 3C). The changes in thymi of glioma-bearing mice were highly consistent when compared to PBS-injected mice (Supplementary Fig. 1B), while the two control groups had similar transcriptomes (Supplementary Fig. 1C). Strongly and significantly regulated genes include Serpina3n and genes related to the complement pathway (Fig. 3C).

Epithelial cells are likely not affected by glioma-induced thymic involution

We next sought to evaluate whether epithelial cells in the thymi of GL261-bearing mice were decreased compared to controls. We focused on two widely expressed epithelial cell-specific genes Epcam and Aire (Supplementary Fig. 1D). We did not observe a decline in expression levels of these genes in thymi of glioma-bearing mice compared to controls (Supplementary Fig. 1D). This contrasts with expression patterns observed in two T cell lineage-specific genes Thy1 and Rag2, which are significantly downregulated in thymi of glioma-bearing mice compared to controls (Supplementary Fig. 1E). Next, we confirmed lack of epithelial cell loss in

Figure 1 Continued

by placing a circular region of interest over the head. Mice with bioluminescence intensities above 10^5 (photon/s) were considered to be tumour-bearing whereas those below 10^5 (photon/s) were considered to be tumour-negative. (**I**) Thymic weight and (**J**) cellularity are compared between PBS-injected and B16-F1 melanoma implanted mice on Day 11 when B16-F1 implanted mice became moribund. (**K and L**) Similar to the thymus, spleens of glioma-bearing mice (GL261-Luc implanted) are significantly reduced in size when compared to naïve unmanipulated controls (**K**, weight; **L**, cellularity). (**M**) Experimental design for implantation and analysis of RCAS-bearing spontaneous gliomas is shown. Briefly, DF1 chicken fibroblasts cultured in DMEM with 10% FBS at 39°C and 5% CO_2 were transfected with RCAS vectors (PDGFb, H3.3K27M, and Cre recombinase). After 2–3 weeks of passaging, 10^5 DF1 cells with a 1:1:1 vector ratio or untransfected DF1controls were implanted into the brainstems of postnatal Day P3-P5 Nestin Tv-a, p53$^{fl/fl}$ pups. In this model, 3–5-day-old mice were intracranially injected with cells that can induce spontaneous glioma growth in the brain stem. After 28 days, all mice underwent T$_2$-weighted MRI to assess tumour volumes. Mice with detectable tumours and non-tumour-bearing control mice were euthanized for assessment of the thymus. (**N**) Thymic weight and (**O**) cellularity in tumour-negative versus RCAS tumour-bearing is shown. n = 4–8 for RCAS experiments. n = 13–34 in GL261 experiment pooled from three to four independent experiments. n = 5 in B16-F1 experiment. All B16 implanted mice developed detectable tumours. Data are shown as individual mice with mean. Error bars represent standard deviation. Mann-Whitney U-test was used to assess statistical significance. ns: $P \geqslant 0.05$, $*P = 0.01$ to 0.05, $**P = 0.001$ to 0.01, $***P = 0.0001$ to 0.001, $****P < 0.0001$.
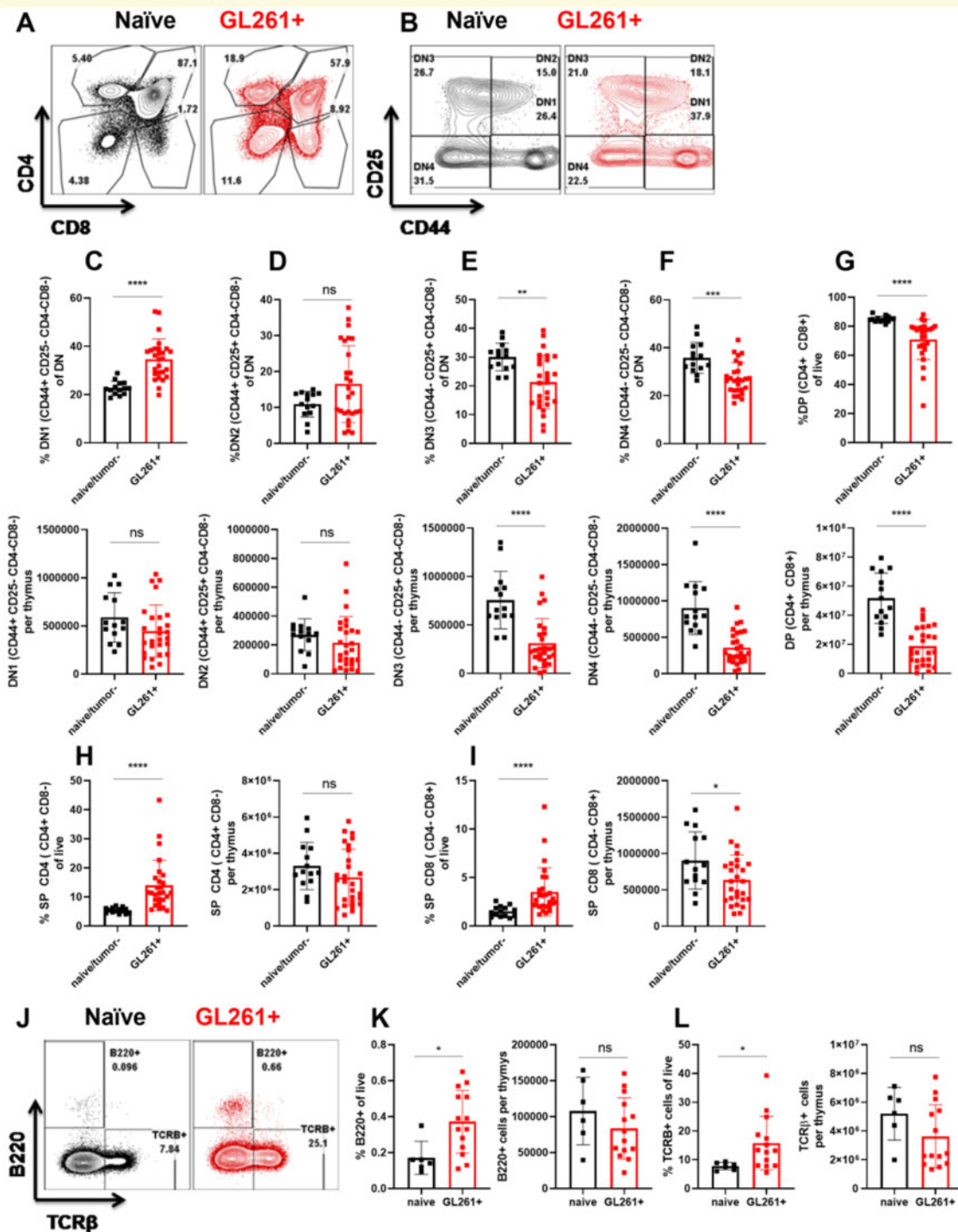
Figure 2 Brain tumours induce changes within the thymus that dysregulate T-cell development. (**A** and **B**) Gating strategy is shown using representative naïve and glioma-bearing mice. (**A**) Following gating on singlets, live, and CD45$^+$ cells, we used CD4 and CD8 parameters to determine double-negative (DN), double-positive (DP), SP4 (single-positive CD4), and SP8 (single-positive CD8) T cells. (**B**) We then focused on the double-negative gate to define DN1–4 populations. DN1 is defined as CD44$^+$CD25$^-$, DN2 is defined as CD44$^+$CD25$^+$, DN3 is defined as CD44$^-$CD25$^+$, and DN4 is defined as CD44$^-$CD25$^-$ populations within the double-negative gate. (**C–G**) Frequencies (*top*) and numbers (*bottom*) of DN1–DN4 and double-positive cells are quantified between naïve or tumour (−), and glioma-bearing mice. (**H** and **I**) Frequencies and numbers of single-positive CD4 and CD8 T cells are quantified. *n* = 14–27. Data are shown as individual mice with mean. Data are pooled from two independent experiments. This experiment was repeated five times and similar results were obtained. Error bars represent standard deviation. Mann-Whitney U-test was used to assess statistical significance. ns: $P \geqslant 0.05$, *$P = 0.01$ to 0.05, **$P = 0.001$ to 0.01, ***$P = 0.0001$ to 0.001, ****$P < 0.0001$. (**J**) Post selection TCRβ$^+$ cells and B220$^+$ B cells within the thymus are increased in glioma-bearing mice compared to controls. (**K**) Frequencies and numbers of thymic B cells are quantified. (**L**) Frequencies and numbers of TCRβ$^+$ cells in the thymus are quantified. *n* = 6–14. Data are shown as individual mice with mean. Error bars represent standard deviation. Mann-Whitney U-test was used to assess statistical significance. ns: $P \geqslant 0.05$, *$P = 0.01$ to 0.05, **$P = 0.001$ to 0.01, ***$P = 0.0001$ to 0.001, ****$P < 0.0001$.
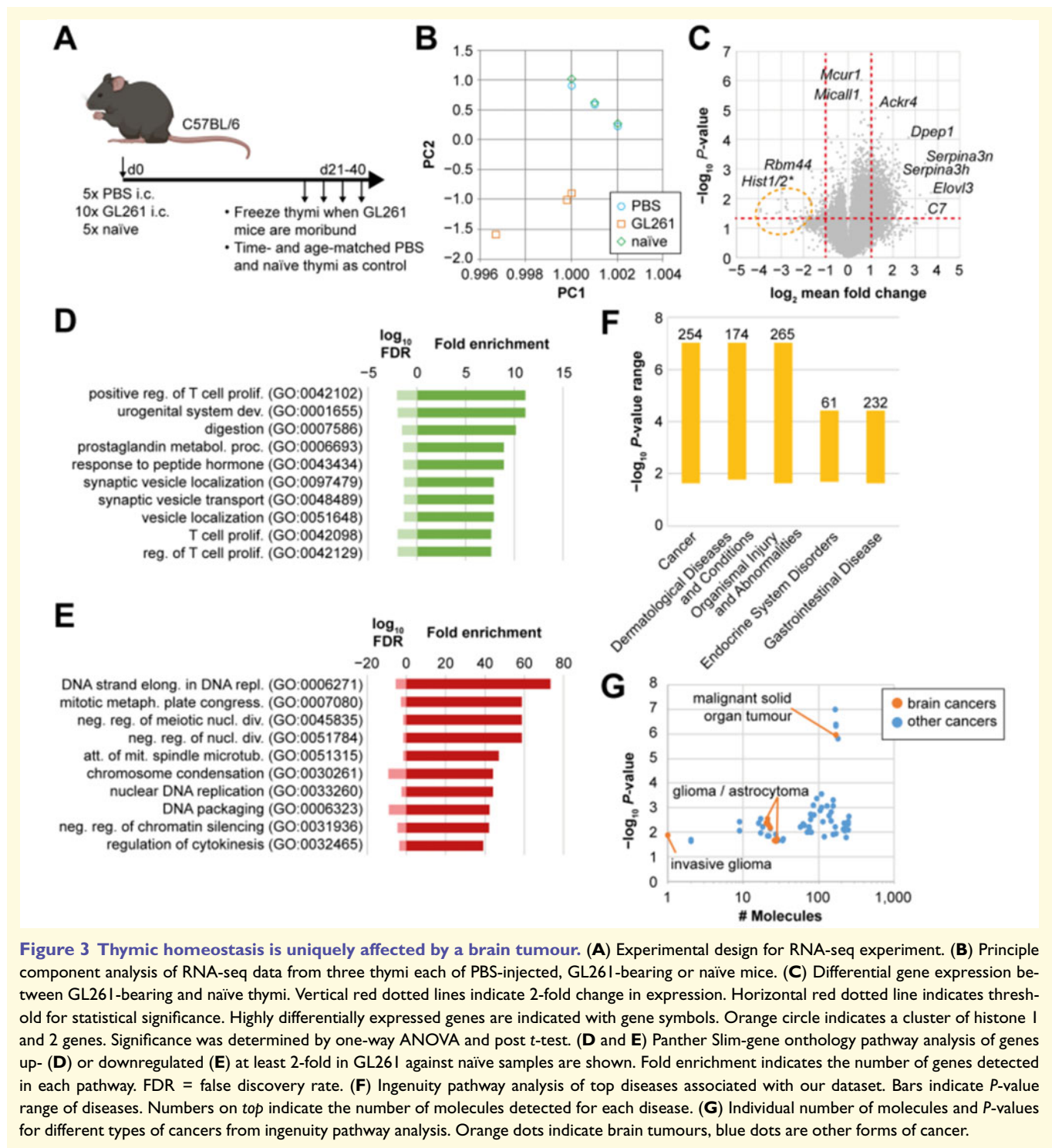
Figure 3 Thymic homeostasis is uniquely affected by a brain tumour. (**A**) Experimental design for RNA-seq experiment. (**B**) Principle component analysis of RNA-seq data from three thymi each of PBS-injected, GL261-bearing or naïve mice. (**C**) Differential gene expression between GL261-bearing and naïve thymi. Vertical red dotted lines indicate 2-fold change in expression. Horizontal red dotted line indicates threshold for statistical significance. Highly differentially expressed genes are indicated with gene symbols. Orange circle indicates a cluster of histone 1 and 2 genes. Significance was determined by one-way ANOVA and post t-test. (**D** and **E**) Panther Slim-gene ontology pathway analysis of genes up- (**D**) or downregulated (**E**) at least 2-fold in GL261 against naïve samples are shown. Fold enrichment indicates the number of genes detected in each pathway. FDR = false discovery rate. (**F**) Ingenuity pathway analysis of top diseases associated with our dataset. Bars indicate P-value range of diseases. Numbers on *top* indicate the number of molecules detected for each disease. (**G**) Individual number of molecules and P-values for different types of cancers from ingenuity pathway analysis. Orange dots indicate brain tumours, blue dots are other forms of cancer.

atrophied thymi of glioma-bearing mice compared to controls using flow cytometry (Supplementary Fig. 1F–H). We determined total numbers of CD45-, EPCAM-expressing CD45-, and MHCII expressing EPCAM-expressing cells within the thymus to be comparable between naïve and glioma-bearing mice (Supplementary Fig. 1F–H). These data suggest that epithelial cells are likely not affected by glioma-induced changes in the thymus.

Gene expression during thymic involution is inconsistent with changes induced by stress responses

We next determined biological pathways with enriched genes from our dataset using unbiased approaches. GO analysis of highly upregulated genes (>2-fold in GL261 compared to naïve) identified pathways associated with T-cell

proliferation, suggesting subsets within the thymus are striving to proliferate and maintain cellularity (Fig. 3D). In contrast, pathways that were significantly downregulated included DNA replication and elongation suggesting a possible block in proliferation for other subsets (Fig. 3E). Next, we evaluated top pathways regulated in our dataset as predicted by IPA (Supplementary Fig. 1I and J). Interestingly, genes associated with glucocorticoid receptor signalling, part of the acute response pathway, were not significantly enriched in our dataset (Supplementary Fig. 1I) suggesting minimal role for stress-induced pathways. Instead, genes enriched in this pathway included those encoding Serpina3, Serpina1, Il1 signalling, haptoglobin, and fibrinogen (Supplementary Fig. 1I).

Finally, we used IPA to determine the likelihood that our dataset is associated with particular diseases. Interestingly, analysis of our thymic bulk RNA-seq data from mice with brain gliomas indicated cancer to be the top disease associated with our dataset (Fig. 3F). In fact, ~254 molecules that are known to regulate cancer development and prognosis were significantly enriched in our thymic RNA dataset (Fig. 3F). Among cancers linked to our dataset, those affecting the CNS including gliomas, and astrocytomas were highly enriched (Fig. 3G). These data suggest that GBM is a systemic disease that uniquely alters thymic homeostasis in a brain-cancer-specific manner.

Mice harbouring GL261 gliomas exhibit peripheral immunosuppression consistent with glioblastoma patients

We have demonstrated that chronic neurological insults including experimental GBM cause thymic (and splenic) involution. We next investigated if thymic involution occurs concurrently with peripheral immunosuppression affecting other immune organs. Patients with GBM often present with low CD4 T-cell counts and reduced expression of MHCII on their peripheral blood monocytes (Gustafson et al., 2010; Chongsathidkiet et al., 2018). Additionally, increased T-cell sequestration in the bone marrow and loss of spleen volume was recently reported in patients with GBM (Chongsathidkiet et al., 2018). Because patients with GBM have this distinct peripheral immunosuppression phenotype, we further assessed the peripheral immune system in the GL261 model. In mice inoculated with GL261 gliomas, we observed a continuous decline in blood CD4 and CD8 T cells (Fig. 4A, C, D and Supplementary Fig. 2B and C). By bleeding the same tumour-bearing mouse weekly (and naïve mice as controls), we were able to observe an overall decline in CD4 T cells as glioma-bearing mice became moribund (Fig. 4A and Supplementary Fig. 2A, showing two mice; the first died on Day 14 and the second died on Day 21 post tumour inoculation). The drop in frequencies of CD4 and CD8 T cells in GL261 glioma-bearing mice translated into reduced T-cell counts as total numbers of cells per 100 µl of

blood remained comparable between control and GL261-bearing mice (Fig. 4G, H and Supplementary Fig. 2D). In Fig. 4G–L, data are obtained at end point when glioma-bearing mice are moribund. Declines in frequencies and numbers of B cells in blood did not reach statistical significance (Supplementary Fig. 2E).

We next evaluated MHCII expression in GL261 glioma-harbouring mice. Similar to T-cell counts, a drop in MHCII expression and total counts of MHCII-positive cells was apparent in all CD45$^+$ leucocytes in blood (Fig. 4B, E, J and K). Importantly, this drop in MHCII expression correlated with tumour-burden on Day 28 as mice with the highest tumour-burden had the lowest levels of MHCII expression on blood CD45$^+$ leucocytes (Fig. 4F). This decline in MHCII was also apparent when separately analysing B cells in the blood (Fig. 4L). MHCII$^{-/-}$ mice had higher tumour incidence post implantation with GL261 cells (data not shown) and lower survival compared to wild-type counterparts (Supplementary Fig. 2I and J). This suggests that MHCII downregulation may be a crucial mechanism of immunosuppression in GBM.

Next, we sought to address whether T-cell counts decline in the spleen of glioma-bearing mice compared to controls. Similar to blood, we found reductions in total numbers of CD45$^+$ cells, CD4 T cells, CD8 T cells, and B cells while the frequencies of these populations did not change (Fig. 4M–O and Supplementary Fig. 2G and H). This is consistent with the reported literature in the CTIIA glioma model (Chongsathidkiet et al., 2018). Additionally, we observed reduced counts of MHCII$^+$CD45$^+$, MHCII$^+$ B cells and MHCII$^+$CD11b$^+$ monocytes and macrophages (Fig. 4N–P). We observed a reduction in frequency of MHCII-expressing CD45$^+$ cells, and B cells, but not CD11b$^+$ cells (Fig. 4N–P).

Finally, we evaluated bone marrow of glioma-bearing mice for evidence of T-cell sequestration as reported in patients with GBM and CTIIA glioma-bearing mice (Chongsathidkiet et al., 2018). As expected, we observed a significant, but modest, increase in frequency of T cells within the bone marrow of glioma-bearing mice compared to controls (Supplementary Fig. 3A and B). We next sought to determine the specific phenotype of sequestered T cells within the bone marrow of glioma-bearing mice. We evaluated whether an analogous increase was observed in CD4 and CD8 compartments within the bone marrow of glioma-bearing mice compared to controls. We found that only the effect on CD4 T cells reached statistical significance (Supplementary Fig. 3C and D). We next investigated the specific population of CD4 T cells that accumulate in the bone marrow of glioma-bearing mice. We determined that bone marrow harbours populations of CD62L$^+$CD69$^-$ CD4 T cells at baseline (Supplementary Fig. 3E and F). Interestingly, this same population is expanded in glioma-bearing mice when compared to naïve controls (Supplementary Fig. 3E and F). We did not observe a significant increase in total cellularity of bone marrow in glioma-bearing mice compared to controls indicating a preferential increase in T cells (Supplementary Fig. 3G). Numbers or
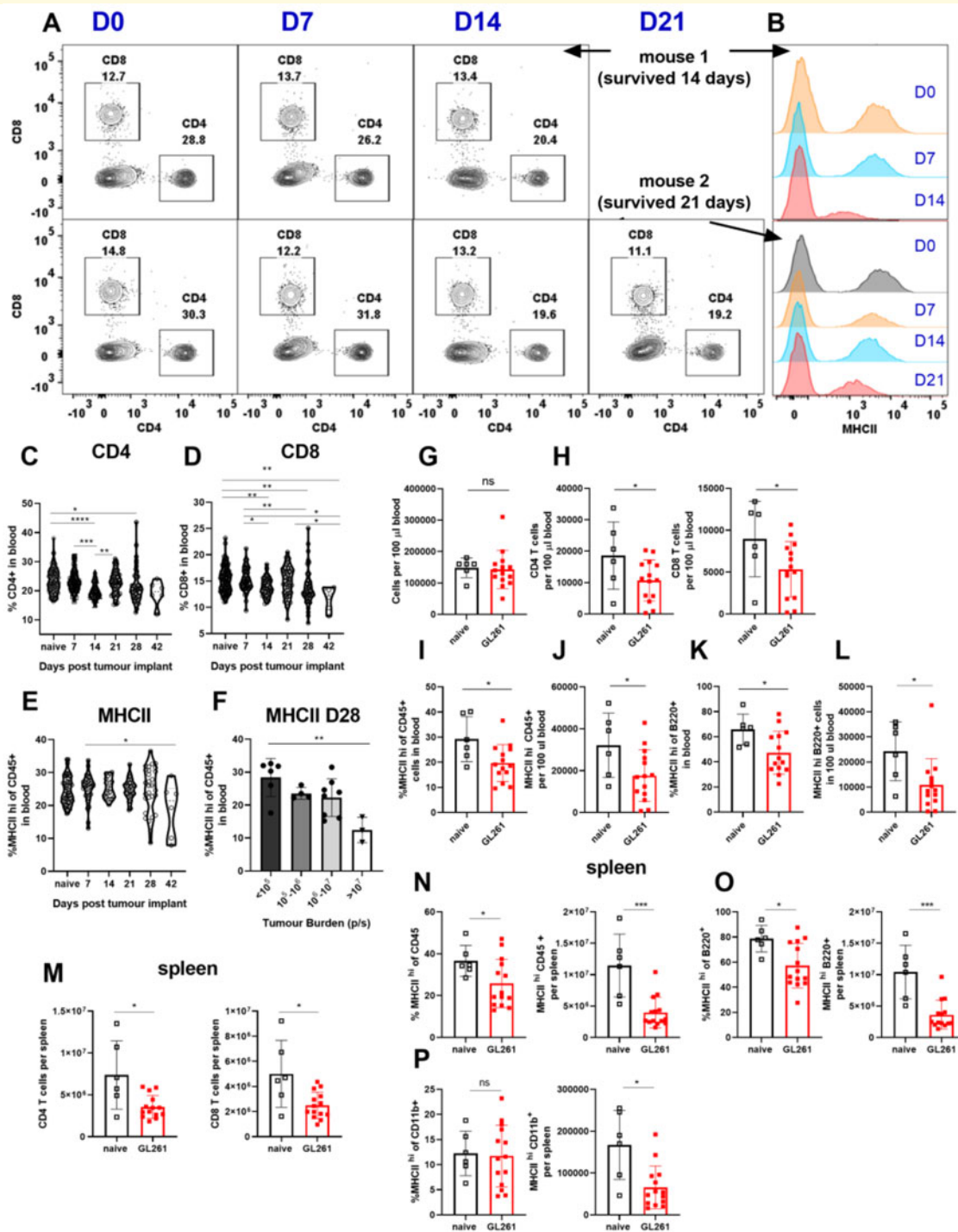
Figure 4 Mice harbouring GL261 gliomas exhibit peripheral immunosuppression consistent with patients with GBM. (**A**) CD4 and CD8 T-cell levels are tracked through weekly bleeding in individual mice. (**B**) MHCII expression on all CD45$^+$ cells in blood is tracked weekly in individual mice. (**C** and **D**) Two representative mice are shown. (**C**) Frequencies of CD4 and (**D**) CD8 and (**E**) MHCII expression on CD45$^+$ cells in blood are tracked across GL261 implanted mice through weekly bleeding (*n* = 6–124). Data are pooled from four to five independent experiments. (**I**) Variability in MHCII expression on blood CD45$^+$ cells on Day 28 is plotted as a function of tumour burden as measured by bioluminescence intensity (*n* = 3–8) data are pooled from two independent experiments. (**G**) Total cells per 100 μl of blood do not change between naïve and glioma bearing mice. Blood comparisons in **G–L** are made at times when GL261-bearing mice became moribund. (**H**) Reduction in frequency of CD4 and CD8 T cells translates into a reduction in total counts of CD4 and CD8 T cells in blood. (**I**) Frequency and (**J**) number of CD45$^+$ cells in blood with high expression of MHCII is quantified. Similarly, (**K**) frequency and (**L**) numbers of B cells with high levels of MHCII expression in blood are decreased in glioma-bearing mice compared to controls. (**M**) Numbers of CD4, and CD8 T cells, and (**N**) frequencies and numbers of MHCII^{hi} CD45$^+$, (**O**) MHCII^{hi} B cells, and (**P**) counts of MHCII^{hi} CD11b$^+$ cells are compared between glioma-bearing and naïve mice in the spleen. For T-cell gating: we gated on singlets, live, CD45$^+$, TCRβ$^+$ B220$^-$, CD4$^+$ or CD8$^+$ cells. For B-cell gating, we used singlets,

(continued)

frequencies of B220$^+$ cells in the bone marrow did not change between naïve and glioma-bearing mice (Supplementary Fig. 3H). Numbers of CD11b$^+$ cells within the bone marrow of glioma-bearing mice did not increase significantly while their frequency increased (Supplementary Fig. 3I). Therefore, GL261-harbouring mice exhibit features of peripheral immunosuppression similar to patients with GBM. Hence this model is valuable in studying mechanisms of immunosuppression in GBM.

Circulating factors in glioma-bearing mice are responsible for inducing some features of immunosuppression

To determine the potential role of blood-derived factors in inducing immunosuppression in glioma-bearing mice, we used parabiosis. We surgically joined GFP-expressing C57BL/6 to wild-type C57BL/6 mice. Sharing of blood circulation was confirmed by gross visualization of shared blood vessels and presence of GFP$^+$ cells in blood of both parabionts prior to tumour implantation and throughout the duration of the experiment (Fig. 5A, Supplementary Figs 4F and 5C). One month post parabiosis surgery, the GFP-expressing mouse was intracranially inoculated with GL261 glioma cells (Fig. 5A). The non-metastatic nature of this tumour was confirmed by bioluminescence imaging (Fig. 5B and Supplementary Fig. 4A). Interestingly, having two conjoined immune systems did not induce early tumour rejection, as parabiotic mice became moribund with similar kinetics to individual glioma-bearing mice (Supplementary Fig. 4B). We next asked if hallmark features of GBM were present in both glioma-bearing and non-tumour-bearing parabionts. Our analysis revealed that peripheral blood CD4 T-cell counts and MHCII expression levels on blood CD45$^+$ cells were reduced in both tumour-free and tumour-bearing parabionts (Fig. 5C, D and Supplementary Fig. 4C–E). Next, we asked if thymic involution occurs in both thymi as a result of sharing circulation. Thymi isolated from both glioma-bearing and tumour-free parabionts were significantly smaller as evidenced by both lower weight and cellularity compared to naïve-naïve parabionts and age-matched naïve historical controls (Fig. 5E, Supplementary Fig. 5A and B). Parabiosis of naïve-to-naïve mice did not results in thymic involution, declines in blood T-cell counts, or decreased MHCII expression on blood CD45$^+$ leucocytes (Supplementary Fig. 5D and E). Together, these data demonstrate that exposure to the circulation of a

GL261-tumour-bearing mouse is sufficient to induce thymic involution and reductions in T-cell counts and MHCII expression in tumour-free mice in the absence of brain injury.

T-cell sequestration in the bone marrow of glioma-bearing mice is not mediated through soluble factors

We next sought to determine if the bone marrow specific facet of immunosuppression during glioma progression is transferable via soluble factors. We performed parabiosis and evaluated frequencies and total numbers of T cells in the bone marrow of glioma-bearing and tumour-free parabionts compared with naïve-to-naïve parabionts. As shown in Fig. 5F, T-cell sequestration in the bone marrow only occurs in the glioma-bearing parabiont and not in the attached tumour-free parabiont. We also evaluated the phenotype of bone marrow resident T cells in both sets of parabionts. Interestingly, the bone marrow of mice with no brain tumours are composed mainly of CD44^{hi}CD62L$^+$ central memory T cells, while naïve T cells are a minor population (Fig. 5G). We found a reduction in central memory T cells concurrently with increased frequencies of naïve T cells in bone marrows of both glioma-bearing and tumour-free parabionts when compared to naïve-naïve parabiotic pairs (Fig. 5G). This shift towards retention of naïve T cells in the bone marrow was evident in glioma-bearing non-parabiotic mice as well (Supplementary Fig. 3E and F). Hence, exposure to the circulation of tumour-bearing mice is sufficient to induce a shift towards naïve T cells and a reduction in central memory T cells in the bone marrow. This occurred despite the absence of increased T-cell sequestration in the bone marrow of tumour-free mouse.

Serum isolated from GL261 glioma-bearing mice suppresses T-cell proliferation *in vitro*

Parabiosis revealed that soluble factors in circulation are sufficient to induce several facets of immunosuppression observed during glioma progression. Next, we asked if serum obtained from GL261-glioma-bearing mice suppresses T-cell proliferation *in vitro*. We cultured CFSE-labelled T cells isolated from naïve mice in the presence of anti-CD3/CD28 beads, which induce strong antigen-independent proliferation. This stimulation results in robust activation and proliferation of both CD4 and CD8 T cells, which is evident

Figure 4 Continued
live, CD45$^+$, or TCRβ$^-$B220$^+$ cells. For CD11b gating, we used singlets, live, CD45$^+$, TCRβ$^-$B220$^-$, or CD11b$^+$ cells. Data are shown as individual mice with mean. Error bars represent standard deviation. One-way ANOVA with Tukey's multiple comparisons test was used to assess statistical significance for **C–F**. Mann-Whitney U-test was used to assess statistical significance in **G–P**. ns: $P \geqslant 0.05$, *$P = 0.01$ to 0.05, **$P = 0.001$ to 0.01, ***$P = 0.0001$ to 0.001, ****$P < 0.0001$.
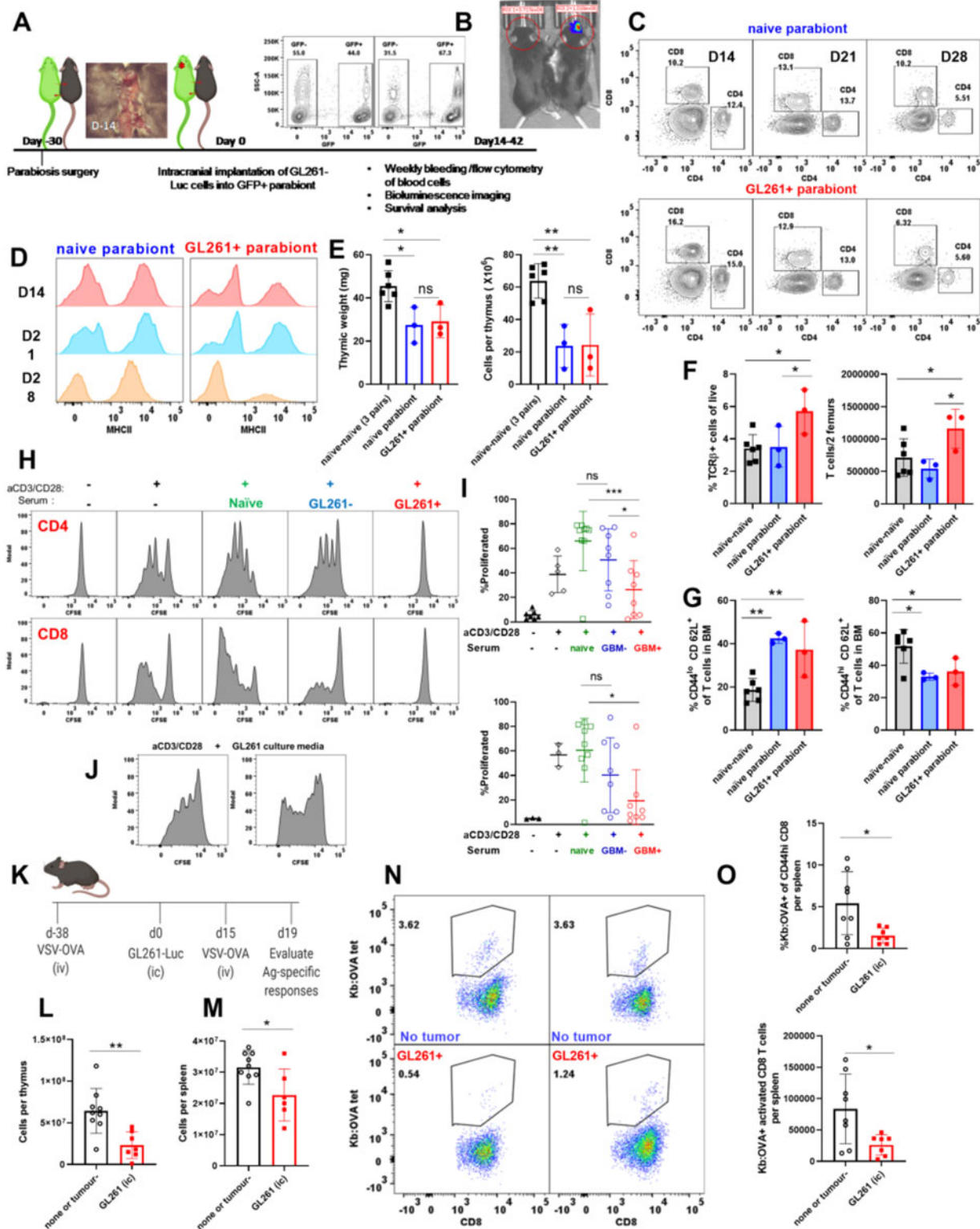
Figure 5 Multifaceted systemic immunosuppression in glioma-bearing mice involves release of immunosuppressive soluble factors. (**A**) Schematic of parabiosis and verification of sharing of vasculature and GFP^{+} cells are shown. (**B**) Tumour burden is shown in the tumour-bearing parabiont compared to the tumour-free partner. (**C**) A representative flow plot of blood CD4 and CD8 frequencies is shown in both parabionts from three consecutive weeks post tumour implant. (**D**) MHCII expression on CD45^{+} cells in the blood is shown from three consecutive bleeds. (**E**) Thymi from naïve and glioma-bearing parabionts are compared to naïve-to-naïve parabionts. (**E**, *left*) Thymic weight and (**E**, *right*) cellularity is compared between naïve-to-naïve and naïve-to-tumour-bearing parabionts. (**F**) Parabiosis of a tumour-bearing to a non-tumour-bearing mouse revealed that T-cell sequestration in the bone marrow only occurs in the GL261 + parabiont and not in the attached tumour-free parabiont. (**G**) However, phenotype of bone marrow resident T cells changes in both tumour-bearing and tumour-free parabionts

(continued)

by dilution of the CFSE dye (Fig. 5H and I). To these cultures we added 5% serum isolated from naïve, GL261 tumour-bearing, or tumour (–) mice. T-cell proliferation was measured 72-h post-stimulation. Serum of GL261 glioma-bearing mice, but not serum obtained from naïve or tumour (–) mice, inhibited T-cell proliferation *in vitro* (Fig. 5H and I). To distinguish between tumour-derived or host-derived factors, we tested whether the GL261 culture media is capable of inhibiting T-cell proliferation in a similar assay. Supernatant obtained from GL261 culture had no effect on T-cell proliferation (Fig. 5J). These data suggest that immunosuppressive factors in serum of glioma-bearing mice are likely host-derived and not tumour-derived. Although, it remains possible that the immunosuppression in serum affects T cells indirectly through antigen presenting cells.

Glioma-bearing mice are functionally immunosuppressed *in vivo*

Given that serum isolated from glioma-bearing mice potently inhibited T-cell proliferation *in vitro*, we next sought to determine if GBM-bearing mice had measurable defects in T cell functions *in vivo*. We focused on responses of pre-existing memory T cells in glioma-bearing mice exhibiting multi-faceted immunosuppression compared to controls. We asked whether pre-existing memory responses that were generated in the absence of brain tumours were fully functional during glioma progression. To assess memory responses, we infected mice with a VSV vector bearing OVA antigen (VSV-OVA) intravenously 6 weeks prior to GL261 tumour implantation (Fig. 5K). Fifteen days post tumour-implantation, we rechallenged with VSV-OVA and euthanized mice 4 days later (Fig. 5K). We evaluated antigen-specific responses of CD8 T cells using tetramers against OVA (K^b:OVA). We found that glioma-bearing mice with previous memory to VSV-OVA exhibited a reduction in thymic and spleen cellularity that was similar to non-VSV-OVA-immune glioma-bearing mice (Fig. 5L and M). Quantification of K^b:OVA tetramer-positive CD8 T cells revealed a significant reduction in frequencies and numbers of OVA-specific CD8 T cells responding to reinfection in spleens of glioma-bearing mice compared to tumour-free controls (Fig. 5M–O). Together, these data provide evidence of glioma-induced immunosuppression *in vivo* that affects T-cell functions.

Thymic involution is induced following acute neurological insults and is not unique to brain cancers

Experimental models of CNS cancer induce sustained peripheral immunosuppression that affects several immune organs, aspects of which can be mediated through soluble factors. We sought to determine the effect of acute neurological insults on the thymus. To test the effect of acute neurological injuries on thymic homeostasis, we used several models of brain insults. These models included viral infection of the brain, sterile inflammatory injury, physical injury, and seizure inductions (Fig. 6A). The brain is the primary site of insult in all these models. Therefore, effects observed in thymic homeostasis will have originated from the brain insult. To induce a viral infection in the brain, we intracranially infected C57BL/6 mice or SJL mice with 2×10^6 PFU of the neurotropic virus TMEV. TMEV can be cleared effectively in C57BL/6 mice whereas SJL mice experience chronic infection accompanied with demyelination (Huseby Kelcher *et al.*, 2017). TMEV infection resulted in significant and severe thymic involution measurable by a reduction in thymic weight and cellularity 7 days post infection in both C57BL/6 and SJL mice (Fig. 6B). We next investigated if generalized inflammation in the brain could induce thymic involution by intracranially injecting 1 μl of 10 μg/μl LPS into the brain and analysing the thymus 7 days later. We found significant thymic involution in LPS-injected mice compared to naïve unmanipulated controls (Fig. 6C). We next tested the impact

Figure 5 Continued
when compared to naïve-naïve counterparts. Exposure to the circulation of tumour-bearing mouse is sufficient to induce enrichment in naïve L selectin + bone marrow resident T cells in the attached animal with no glioma in the brain. (**H**) Representative histograms depict CD4 (*top*) and CD8 (*bottom*) T-cell proliferation with and without anti-CD3/CD28 Dynabeads in the presence and absence of serum from naïve, tumour (–) and GL261 glioma-bearing mice. To do this assay, T cells from spleens and lymph nodes (inguinal, brachial, and axial lymph nodes) of naïve unmanipulated C57BL/6 mice were isolated and labelled with CFSE. Cells were plated either at 700 000 cells/well in a 96-well plate, or at 1.6×10^6 cells/well in a 24-well plate. Anti-CD3/CD28 beads were added at either 19 μl/well for 96-well plates or at 75 μl/well for 24-well plates. Total volume was 1 ml in 24-well plates and 250 μl in 96-well plates. To these cultures, we added 12.5μl of serum isolated from experimental mice to 96-well plates or 50 μl of serum in 24-well plates. CFSE dilution was assessed using flow cytometry 72 h later. CFSE dilution is shown. (**I**) Per cent cells with CFSE dilution is quantified as a measure of proliferation for each condition. (**I**, *top*) shows quantification for CD4 T-cells and (**I**, *bottom*) indicates CD8 quantification. (**J**) GL261 cell culture media is shown to not prevent T-cell proliferation. (**K**) Experimental design is shown for evaluation of memory responses generated against VSV-OVA during glioma progression. (**L**) Thymic and splenic (**M**) cellularity decreased in glioma-bearing mice previously infected with VSV-OVA compared to mice with no brain injury or tumour (–) controls. (**N** and **O**) Frequencies and numbers of K^b:OVA tetramer + CD8 T cells are quantified in spleens of glioma-bearing and control mice 4 days post VSV-OVA rechallenge. One-way ANOVA with Tukey's multiple comparisons test was used to assess statistical significance for groups larger than two. For comparisons between two groups, Mann-Whitney U-test was used. For **F** and **G**, one-way ANOVA was performed and then an uncorrected Fisher's LSD test was used to compare selected pairs. ns: $P \geqslant 0.05$, *$P = 0.01$ to 0.05, **$P = 0.001$ to 0.01, ***$P = 0.0001$ to 0.001, ****$P < 0.0001$. BM = bone marrow.
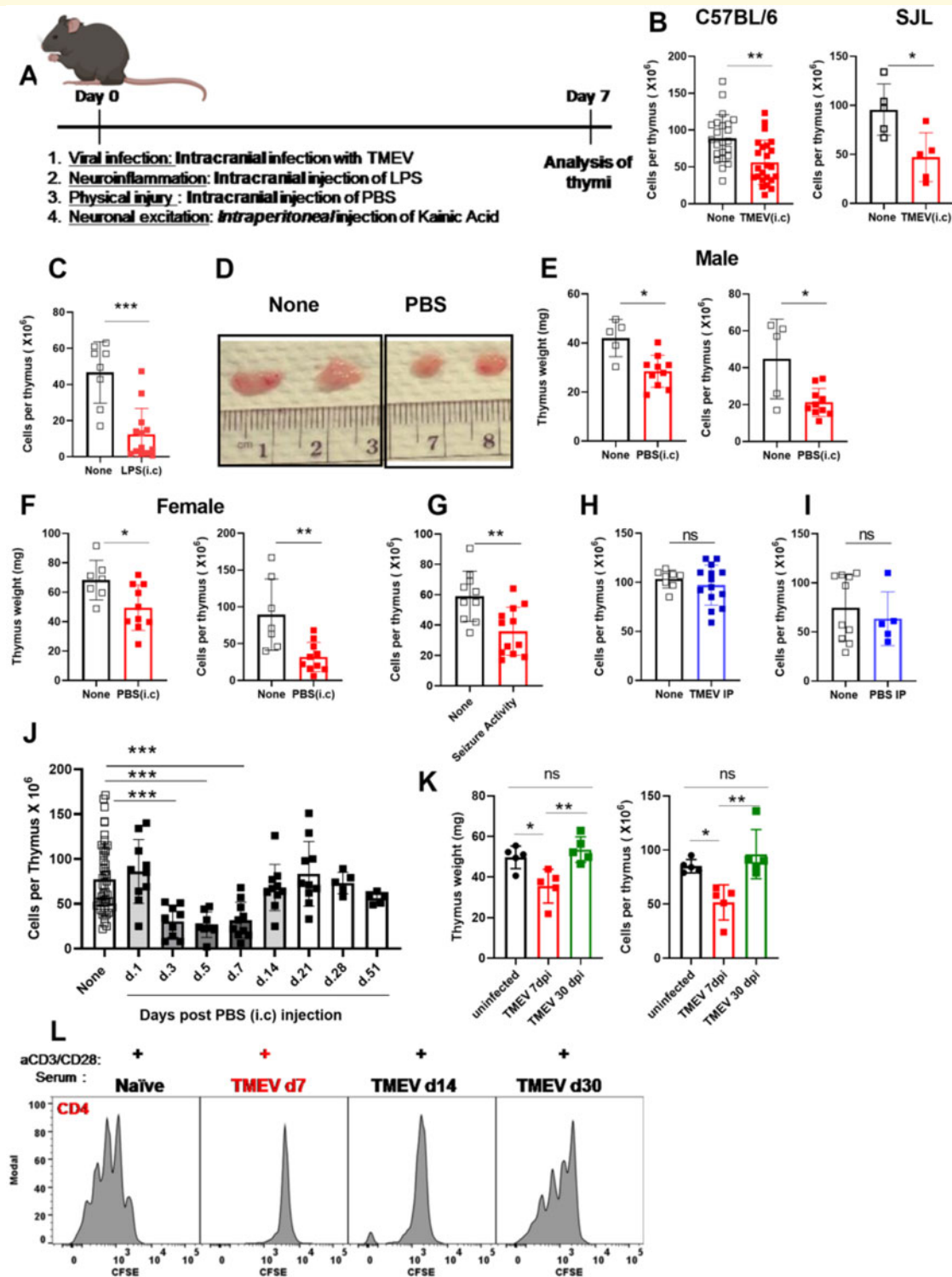
Figure 6 Acute neurological insults with various origins that are delivered to the CNS result in similar thymic involution. (**A**) Experimental design is shown. (**B**) Thymi were analysed on Day 7 post neurological insults. (**B**) Thymic cellularity is quantified in C57BL/6 (*left*) and in SJL mice (*right*) 7 days post TMEV (intracranial, i.c) infection. (**C**) Thymic cellularity is significantly decreased post LPS (i.c.) injection compared to naïve controls. (**D**) Gross comparison of thymi from sham control (PBS i.c) and naïve unmanipulated mice. (**E,** *left*, and **F,** *left*) Thymic weight and cellularity are both significantly reduced in mice injected with PBS (i.c) (**E** and **F**). The decrease in thymic cellularity post PBS injection is reproduced in both male (**E**) and female (**F**) mice. (**G**) Mice injected with KA that had an acute seizure activity measured by Racine's modified scoring system, had a similar thymic involution. In male mice, seizure was induced by injecting 17.5 mg/kg of KA per mouse. In female mice, seizure was induced using 15.5 mg/kg of KA. All mice received valproic acid to stop seizure activity at 90 min post KA injection. Mice injected with KA were scored using a modified Racine score. Mice with scores of 0 were excluded from the study. Fifty per cent of males experienced a stage 4/5 seizure and died within the first hour post KA injection, thus only the remaining mice were used for analysis. Female mice that did not have

(continued)

of a mild physical brain injury on the thymus. To induce physical injury, we intracranially injected 2 μl of sterile PBS into the brain of C57BL/6 mice. We observed significant thymic involution by gross analysis, and reduced thymic weight and cellularity in both male and female mice 7 days post injection (Fig. 6D–F). To test whether brain insults without surgical trauma also cause thymic involution, we used a seizure induction model following intraperitoneal injection of KA. In this model, we found significant thymic involution 7 days post seizure induction in both male and female mice that experienced acute seizure activity (Fig. 6G and Supplementary Fig. 6A–D). We next tested whether viral infections and physical insults in the periphery induce thymic involution. Intraperitoneal TMEV infection or PBS injection did not induce thymic involution (Fig. 6H and I), demonstrating a requirement for direct injury to the brain to induce thymic involution in these models. Overall, these data demonstrate that various acute neurological insults cause thymic involution and this form of immunosuppression is not an exclusive feature of brain cancers.

Thymic involution following acute neurological injuries is reversible upon clearance of the brain insult

To determine whether thymic involution due to acute brain injury was reversible, we used two acute injury models. First, we quantified thymic involution over time following physical injury to the brain via intracranial PBS injection. Second, we evaluated the thymic response following intracranial TMEV infection in C57BL/6 mice before and after viral clearance. Because we did not expect the intracranial PBS injection to have long-lasting effects in the brain, we hence anticipated that the effect on the thymus would be transient. Following intracranial PBS injection, we determined that thymic involution was present acutely, but was completely reversed by 3 weeks post injection (Fig. 6J). Additionally, as mentioned before, RNA-Seq analysis revealed that gene expression patterns of thymi isolated from mice 3–5 weeks post intracranial PBS injection did not significantly differ from naïve controls confirming reversibility of thymic immunosuppression (Fig. 3). Next, we assessed thymi during TMEV infection in C57BL/6 mice. C57BL/6 mice clear TMEV infection within 21–45 days post

infection (McDole et al., 2006; Cumba Garcia et al., 2016; Tsunoda et al., 2016; Huggins et al., 2017; Huseby Kelcher et al., 2017). Because C57BL/6 mice mount an effective antiviral CD8 T-cell response, this model allows us to determine whether thymic involution is reversible upon viral clearance. Thymic involution was not detectable in mice 30 days post TMEV infection and was only observed acutely (Fig. 6K). Together, these data demonstrate that thymic involution due to acute neurological injury is reversible upon clearance of the brain insult.

Sera of mice with on-going acute neurological insults inhibit T-cell proliferation in vitro

We determined that sera isolated from glioma-bearing mice suppress T-cell proliferation in vitro. Therefore, we next assessed whether sera isolated from mice with other neurological insults suppress T-cell function. We cultured naïve T cells with anti CD3/CD28 beads with and without serum isolated from mice post TMEV infection. Mice injected with PBS (intracranially), or B16 melanoma (intracranially) were also assessed using this assay. Serum obtained from TMEV infected mice at acute time points (7 days post injection, dpi), but not at time points post viral clearance (30 dpi), potently inhibited T-cell activation and proliferation in vitro (Fig. 6L, Supplementary Fig. 7B and C). Similarly, serum acquired from PBS injected mice at acute time points was immunosuppressive while serum obtained at late time points did not inhibit T-cell proliferation (Supplementary Fig. 7D). Serum obtained from mice implanted with B16 melanoma had immunosuppressive properties as well (Supplementary Fig. 7A). These data suggest that at the time of confirmed thymic involution, serum harbours a potent immunosuppressive factor capable of inhibiting T-cell proliferation in vitro. Importantly, this factor is no longer present in serum following resolution of neurological insults.

Adrenal glands play a crucial role in maintaining immune organ size at baseline

We next aimed to elucidate whether cortisol and other stress hormones play a significant role as soluble mediators of

---

Figure 6 Continued

any seizure activity by 50 min were injected with an extra 3 mg/kg of KA and their seizure activity was monitored. (H) TMEV infection or (I) PBS injection intraperitoneally (IP) do not induce thymic involution. (J) Thymic involution due to intracranial injection of PBS is reversible. (J) Thymi were harvested at time points post intracranial injection and cellularity was evaluated. (K) Thymic involution following the clearance of TMEV is also reversible. (K, left) Thymic involution as measured by a reduction in thymic cellularity and (K, right) thymic weight is observed on Day 7 post intracranial TMEV infection, but not on Day 30. (L) T-cell proliferation is shown in the presence of serum isolated from TMEV (i.c) infected mice on Days 7, 14 and 30 post infection. n = 5–23 based on the experiment. Graphs show pooled data from two to five independent experiments. Data are shown as individual mice with mean. Error bars represent standard deviation. Mann-Whitney U-test or a one-way ANOVA with Tukey's multiple comparison test was used to assess statistical significance. ns: $P \geqslant 0.05$, *$P = 0.01$ to 0.05, **$P = 0.001$ to 0.01, ***$P = 0.0001$ to 0.001, ****$P < 0.0001$.

peripheral immunosuppression. Cortisol is produced by adrenal glands under the influence of the pituitary (Chen *et al.*, 2016). We purchased commercially-available adult adrenalectomized mice and sought to determine the level of immunosuppression affecting blood, spleen, and thymus in the absence of adrenal glands following intracranial GL261 implantation. Unexpectedly, we found that adrenalectomy alone increases blood, thymus, and spleen cellularity (Fig. 7A–C) in naïve mice. This increase in total cellularity in blood, spleen, and thymus was not due to expansion of particular immune cells as frequencies of T- and B-cell populations appeared comparable between naïve wild-type and adrenalectomized mice (Supplementary Fig. 8A–C, and data not shown). Next, we assessed bone marrow resident T cells in naïve wild-type and adrenalectomized mice. Surprisingly, we found significantly fewer bone marrow resident T cells in naïve adrenalectomized mice compared to controls (Fig. 7D). These data suggest that hormones produced by the adrenal glands in naïve mice play a crucial role in regulating the cellularity of immune organs. This unique homeostatic role of stress hormones has been previously underappreciated. Because of this homeostatic role of adrenal glands in regulating immune organ size, it may be difficult to dissect changes induced due to brain injury from those stemming from lack of the homeostatic role of stress hormones. However, with that caveat in mind, we performed tumour implantations and evaluated various facets of immunosuppression in adrenalectomized GL261 glioma-bearing mice compared to controls. Analysis of peripheral blood revealed that in contrast to glioma-bearing wild-type mice, adrenalectomized mice did not exhibit reductions in T cells, and MHCII expression levels (Fig. 7E–G and Supplementary Fig. 8E–H). Similarly, analysis of thymi from glioma-bearing adrenalectomized mice revealed no evidence of thymic involution or disruptions in T-cell development compared to naïve adrenalectomized controls (Fig. 7H and Supplementary Fig. 8K–M). In spleen, we did not observe evidence of organ atrophy or loss of T cells or MHCII downregulation in glioma-bearing adrenalectomized mice compared to controls (Fig. 7I, Supplementary Fig. 8I and J). The increase in bone marrow resident T cells following glioma implantation did not occur in adrenalectomized mice (Fig. 7J–L) when compared to controls.

Similar to trends observed in the overall T-cell counts within the bone marrow, we observed fewer bone marrow resident CD4 T cells in naïve adrenalectomized mice compared to wild-type controls (Fig. 7M). In contrast to wild-type mice, total frequencies and absolute counts of CD4 T cells did not further increase in adrenalectomized glioma-bearing mice compared to naïve controls (Fig. 7N). Consistent with these trends, we determined that naïve adrenalectomized mice harbour fewer $CD62L^+CD69^+$ CD4 T cells in the bone marrow compared to naïve wild-type mice (Fig. 7O and P). While the increase in $CD62L^+CD69^-$ CD4 T cells in the bone marrow accounted for the observed T-cell accumulation in glioma-bearing wild-type mice (Supplementary Fig. 3E and F), this population did not expand in glioma-bearing adrenalectomized mice (Fig. 7Q).

Serum isolated from glioma-bearing mice harbours a high-molecular-weight immunosuppressive factor

We have thus far determined that serum isolated from glioma-bearing mice is potently immunosuppressive (Fig. 5H and I). Yet, due to the homeostatic role of cortisol at baseline, we were unable to rule out the possibility of steroids as mediators of immunosuppression in serum. Hence, we sought to determine the molecular weight of immunosuppressive molecules found in this serum. Through a series of molecular weight cut-off filtration strategies, we determined that large factors with molecular weights >100 kDa are immunosuppressive and capable of inhibiting T-cell proliferation *in vitro* (Fig. 8A). Small molecules, including species <3 kDa, were not immunosuppressive (Fig. 8A). This finding argues against steroids and small molecules as mediators of immunosuppression. We next sought to validate that cortisol is not responsible for the immunosuppressive properties of serum isolated from glioma-bearing mice. Sera isolated from glioma-bearing wild-type and adrenalectomized mice were equally immunosuppressive *in vitro* (Fig. 8B and C). This is while sera isolated from naïve wild-type or adrenalectomized mice did not affect T-cell proliferation *in vitro* (Fig. 8B and C). Adrenalectomized mice did not have a survival benefit and succumbed to death slightly earlier than wild-type mice (Fig. 8D, MST 23 versus 27).

To conclude, glioma-bearing adrenalectomized mice did not have thymic or spleen involution, a reduction in T-cell counts or reduced MHCII expression (Figs 7 and Supplementary Table 1). However, serum isolated from these mice was as immunosuppressive as serum isolated from glioma-bearing wild-type mice. Furthermore, both normal and adrenalectomized mice succumbed to glioma with similar kinetics (Fig. 8D and Supplementary Table 1). This highlights the importance of counteracting soluble mediators of GBM-induced immunosuppression to improve patient survival.

Discussion

In this study, we analysed both primary and secondary immune organs and describe at least six distinct facets of immunosuppression in experimental GBM: (i) thymic involution associated with a previously unappreciated unique cellular and transcriptomics signature; (ii) spleen involution; (iii) T-cell loss from circulation and secondary lymphoid organs; (iv) MHCII downregulation on leucocytes; (v) release of non-steroid immunosuppressive factors with large molecular weight in serum that inhibit T-cell proliferation; and (vi) phenotypic changes in resident T cells within the bone marrow. These findings demonstrate that brain cancers cause
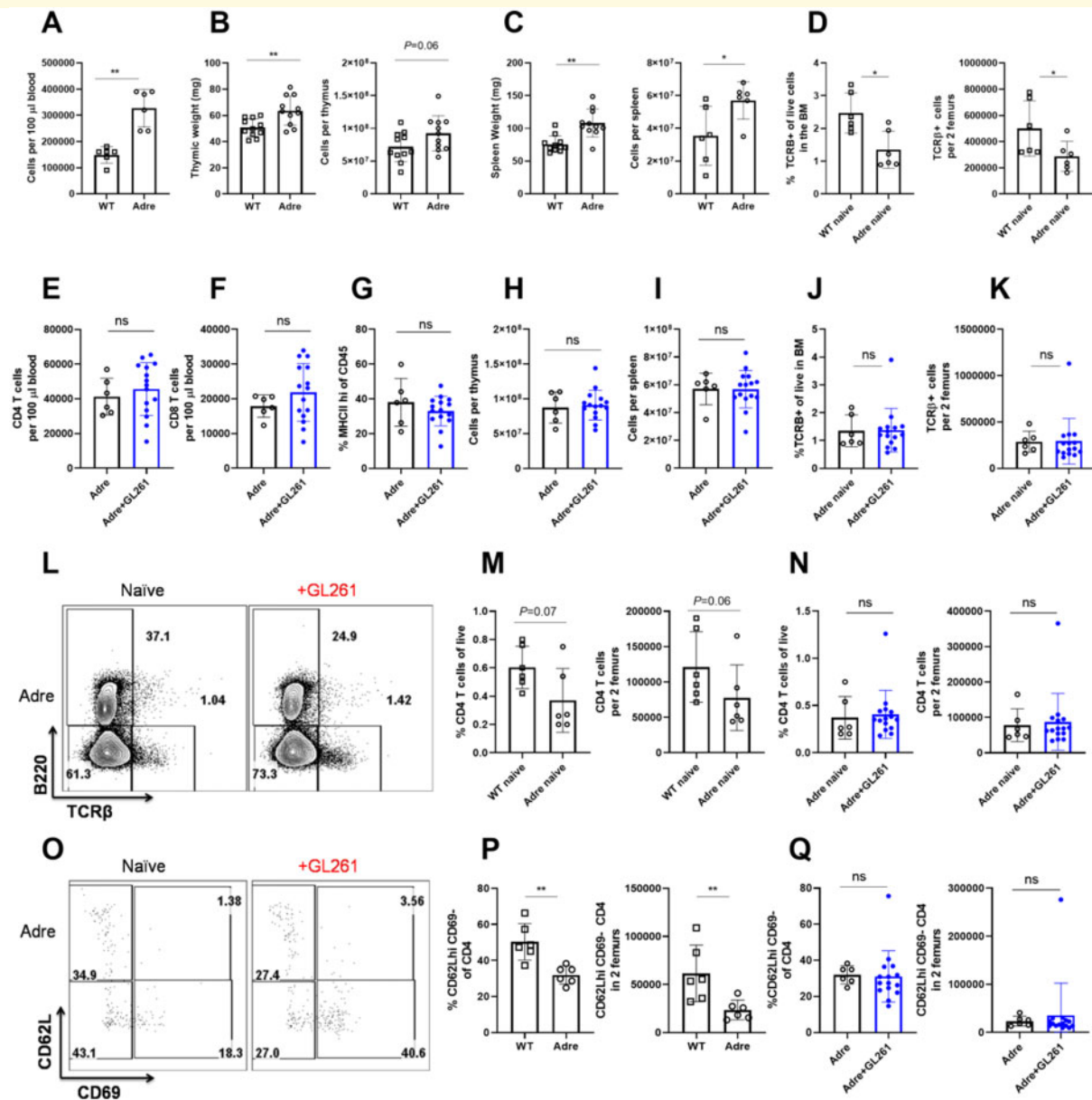
Figure 7 Hormones produced by the adrenal gland control immune organ size and cellularity at baseline. (**A**) Cellularity of blood per equal volume is increased in naïve adrenalectomized mice compared to naïve wild-type (WT) mice. (**B**) Thymic weight and cellularity is increased in naïve adrenalectomized mice compared to naïve wild-type mice. (**C**) Spleen weight and cellularity is increased in naïve adrenalectomized mice compared to naïve wild-type mice. (**D**) Bone marrow of naïve wild-type mice harbour an increased frequency and numbers of T cells when compared to adrenalectomized controls. (**E**) CD4, (**F**) CD8 and (**G**) frequency of MHCII expression on CD45$^+$ cells in blood is equivalent between naïve and glioma-bearing adrenalectomized mice. (**H**) Similarly, cellularity of the thymus and (**I**) spleen does not change in glioma-bearing adrenalectomized mice compared to controls. (**J**) Frequency and (**K**) numbers of bone marrow resident T cells do not increase in glioma-bearing adrenalectomized mice compared to naïve adrenalectomized controls. (**L**) Representative flow plot of T cells within the bone marrow of naïve and glioma-bearing adrenalectomized mice is shown. (**M**) Fewer bone marrow resident CD4 T cells are found in naïve adrenalectomized mice compared to naïve wild-type mice. (**N**) Frequencies and numbers of bone marrow resident CD4 T cells do not increase in glioma-bearing adrenalectomized mice when compared to adrenalectomized naïve controls. (**O**) Phenotype of bone marrow resident CD4 T cells in naïve and glioma-bearing mice reveals enrichment in CD62L$^+$ cells. (**P**) This population is significantly decreased at baseline in naïve adrenalectomized mice when compared to wild-type mice. (**Q**) In contrast to wild-type mice, no increase in CD62L$^+$CD69$^-$CD4$^+$ T cells occurs in the bone marrow of glioma-bearing adrenalectomized mice. $n = 6$–14. Individual data are shown. Error bars represent standard deviation. Mann-Whitney U-test was used. ns: $P \geqslant 0.05$, *$P = 0.01$ to 0.05, **$P = 0.001$ to 0.01, ***$P = 0.0001$ to 0.001, ****$P < 0.0001$.
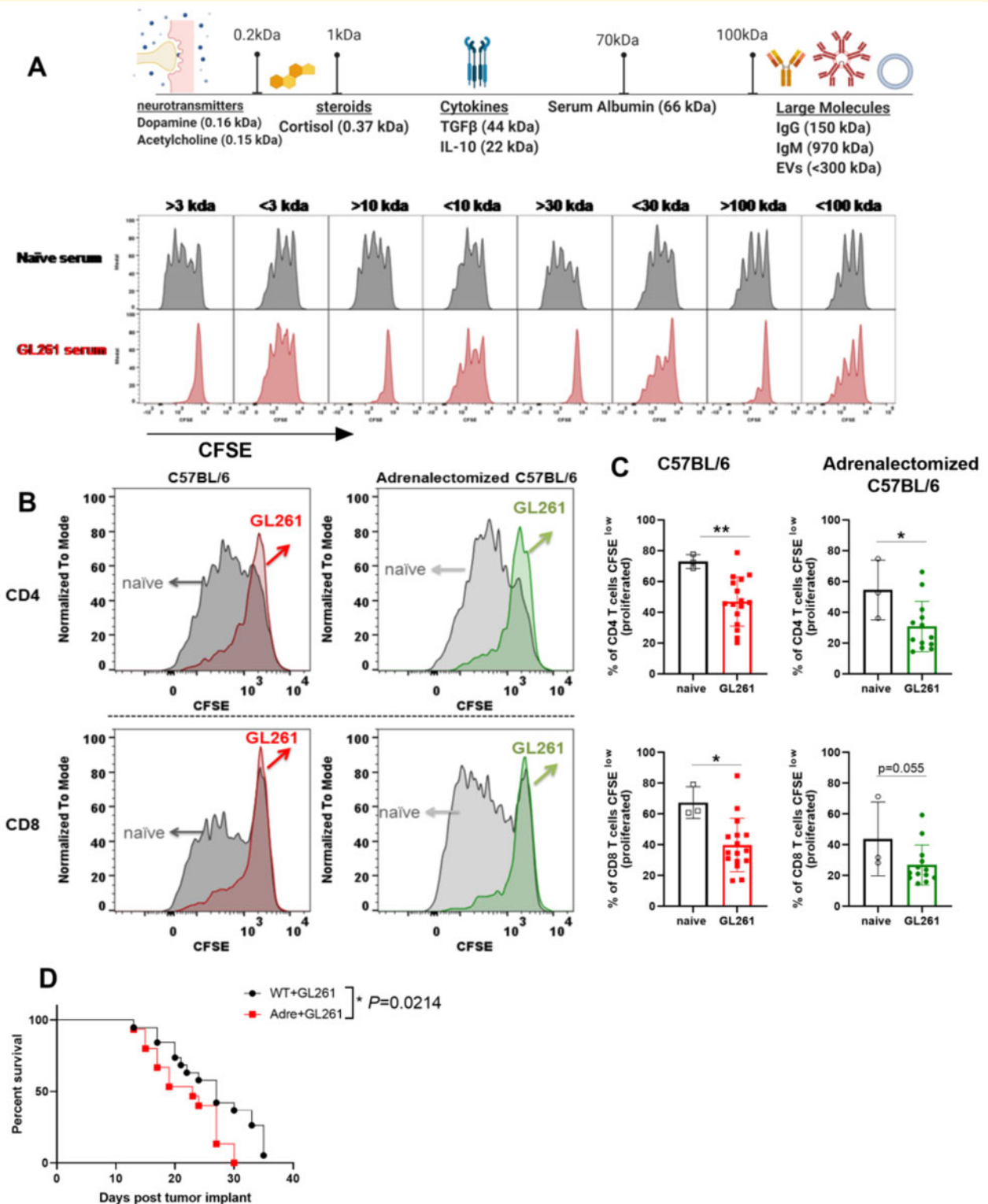
Figure 8 Serum of glioma-bearing mice harbours a novel immunosuppressive factor with molecular weight >100 kD. (**A**) Sera obtained from naïve or glioma-bearing mice were isolated and passed through column-filters with a molecular weight cut-off of 3, 10, 30, or 100 kDa. Both top and bottom fractions were collected and their ability to inhibit T-cell proliferation was tested. T cells obtained from naïve mice were labelled with CFSE and cultured with anti CD3/CD28 Dynabeads in the presence of individual fractions isolated from serum of naïve or glioma-bearing mice. Proliferation was measured 72 h later using flow cytometry. Serum fractions with high molecular weights (>3, >10, >30, >100 kDa) were deemed immunosuppressive as they potently inhibited T-cell proliferation *in vitro*. These data argue against cortisol or other small molecules related to stress hormone pathways playing a role as the immunosuppressive factor produced by the brain during neurological injuries. The molecular weight of the immunosuppressive factor released into serum during neurological injuries is >100 kDa. (**B** and **C**)

(continued)

multifaceted immunosuppression that concurrently affects peripheral blood, serum, bone marrow, thymus, and spleen. Altogether, these effects induce a state of lowered immunity. Our data further demonstrate that immunosuppression due to neurological insults is not exclusive to brain tumours, as it also occurs following several acute neurological insults. This strongly implies immune suppression is generated by the brain and not the individual insult itself. This study also provides detailed analysis regarding the role of stress responses, and non-steroid soluble factors as possible mechanisms ensuing hallmark features of immunosuppression. Further studies are needed and are currently underway in our laboratory to determine whether the multifaceted brain-injury induced immunosuppression of distinct immune organs are interdependent with each other.

Brain injury-induced thymic involution is a significant facet of immunosuppression

Thymic involution leads to lower T-cell production and disruptions in T-cell selection, leading to a lack of adequate peripheral T-cell replenishment when needed. The thymus is reported to shrink following traumatic brain injury (TBI) and experimental GBM in mice (Andaloussi et al., 2008; Chongsathidkiet et al., 2018; Ritzel et al., 2018). However, thymic involution following TBI and GBM has been attributed to the specific pathophysiology of these conditions, rather than an underlying intrinsic peripheral response to brain insults. In contrast to these studies, we report for the first time that thymic involution following brain injury is a pathology-agnostic response with a unique signature. We demonstrated that both acute and chronic neurological injuries of various origins cause thymic involution (Figs 1 and 6). Identical insults induced peripherally did not affect thymic homeostasis (Figs 1 and 6). These findings demonstrate the presence of a brain-thymus communication, which is a feature of neurological injuries.

Our results also support the concept that thymic involution could affect children with diverse brain tumours (including those with benign tumours), altering T-cell repertoire and rendering these patients immunosuppressed for an extended period. Thymic involution is similarly detrimental in adults. The thymus can sense peripheral T-cell numbers and respond by increasing T-cell production if numbers are low (Williams et al., 2007). In the absence of a sudden insult against peripheral T-cells, the thymus may remain small in adults. However, the thymus does not lose its ability to increase in size and generate new T cells during conditions that induce peripheral immunosuppression (Mackall et al., 2001; Weinberg et al., 2001; Williams et al., 2007; Gurkan et al., 2010; van den Broek et al., 2016; Ayasoufi et al., 2017; Rosado-Sanchez et al., 2017). Hence, without a functional thymus, immunosuppression due to brain insults may be detrimental.

While the thymus involutes with brain injury, it returns to baseline homeostasis after the injury is cleared demonstrating thymic plasticity. Thymic recovery is demonstrated by both the recovery of thymic cellularity as well as an enriched recovery signature measured through transcriptional programming in mice with acute reversible brain injuries (Figs 6 and 3). Our study shows that thymic involution and its reversal directly reflect the extent of brain insult and are linked by soluble factors in circulation. Understanding mechanisms of thymic involution and reversal are both important. Inducing thymic reversal may be useful in preventing T-cell immunosuppression during CNS cancers, while also enabling identification of potential therapeutic targets for thymic regeneration. Understanding these immunosuppressive mechanisms offers hope for future paediatric and adult patients with neurological diseases.

The adult thymus is uniquely affected by a CNS tumour

In this study, we demonstrated that transcriptional programming of the thymus was directly altered by a non-metastatic brain tumour in adult mice (Fig. 3). We found epithelial cell development and maturation programs to be enhanced or unaffected, while several T-cell commitment programs were decreased (Fig. 3 and Supplementary Fig. 1, and data not shown). This correlated with a block in T-cell proliferation at the DN2-DN3 stage (Fig. 2). DN2-DN3 stage of T-cell development is associated with high levels of proliferation following TCR β-chain selection (Rothenberg, 2019). A block in DN2-DN3 is likely caused by a block in proliferation, which is consistent with the most downregulated pathways analysed by RNA-seq being involved in DNA replication and cell proliferation (Fig. 3). We also demonstrated that thymic involution was caused by circulating factors using parabiosis (Fig. 5). Confirming this result, serum obtained from mice with various neurological insults potently inhibited activation and proliferation of T cells in vitro at the time of established thymic involution (Figs 5 and 6).

Figure 8 Continued
Consistent with this, we tested the serum obtained from glioma-bearing wild-type (WT) or adrenalectomized mice. Serum isolated from glioma-bearing wild-type and adrenalectomized mice inhibited T-cell proliferation in vitro. (D) Glioma-bearing adrenalectomized mice did not have a survival benefit over wild-type mice despite lacking several facets of immunosuppression. For A, sera obtained from 10 GL261-bearing mice were pooled for analysis. For B and C, $n = 3–10$. Data are shown as individual mice with mean. Error bars represent standard deviation. Mann-Whitney U-test was used to assess statistical significance. ns: $P \geqslant 0.05$, $*P = 0.01$ to 0.05, $**P = 0.001$ to 0.01, $***P = 0.0001$ to 0.001, $****$ $P < 0.0001$.

Given that thymic involution can be transferred through serum-derived soluble factors released during neurological injuries that are potent inhibitors of cell proliferation, it is possible that these factors intervene at the DN2-DN3 stage of T-cell development. We also found an increase in total TCRβ[+] single-positive T cells in the thymus (Fig. 2). Alternatively, the reduced DN3 numbers and enhanced single-positive T cells in the thymus may be explained by accelerated T-cell development.

Thymic involution resulting from experimental glioblastoma is distinct from stress induced involution

Thymic involution and stress responses have historically been linked (Gruver and Sempowski, 2008). We found a significant decrease in double-positive cells in the thymus while single-positive cells appeared to be accumulating within the thymus (Fig. 2). This is interesting as a decrease in double-positive cells due to cell death can be explained by high cortisol levels during stress responses (Verinaud *et al.*, 1998; Gruver and Sempowski, 2008; Zook *et al.*, 2011; Chen *et al.*, 2016). However, brain injury-induced effects on double-positive cells is likely not due to stress hormones alone because first, we did not observe enrichment of genes involved in stress responses or genes involved in glucocorticoid receptor activation in thymic RNA-seq dataset. Instead, highly enriched genes (*Serpina3n*, and genes in complement pathway; Fig. 3) were implicated mainly in pathology of neurological diseases including pain, peripheral nerve damage, and recently in Alzheimer's disease (Takamiya *et al.*, 2002; Hsu *et al.*, 2014; Haile *et al.*, 2015; Vicuna *et al.*, 2015; Sergi *et al.*, 2018; Zhou *et al.*, 2020). Second, we did not observe activation or enrichment of genes associated with the glucocorticoid pathway in our RNA-seq dataset. Finally, concurrent with a loss in double-positive cells, we observed a block in DN2-DN3 stages of development and accumulation of single-positive T cells and B cells in the thymus. The DN2-DN3 block, increased single-positive T cell, and B-cell accumulation signatures in summation are not associated with stress induced, infection induced, or ageing-mediated thymic involution (Godfraind *et al.*, 1995; Godfraind and Coutelier, 1998; Verinaud *et al.*, 1998; Tibbetts *et al.*, 1999; Gruver and Sempowski, 2008; Zook *et al.*, 2011; Chen *et al.*, 2016; Youm *et al.*, 2016; Ayasoufi *et al.*, 2019).

Immunosuppression affecting blood and spleen are additional facets of immunosuppression in glioma-bearing mice

We found a significant loss of T cells and decline of MHCII expression on leucocytes in blood (Fig. 4). These immunosuppressive features occur concurrently with thymic T-cell dysregulation. These together along with immunosuppressive effects of serum suggest that not only T-cell development in the thymus, but also T-cell activation, clonal expansion and maintenance in the periphery are likely affected in glioma-bearing mice. This state of immunosuppression is extremely detrimental because a continuous loss of T cells from secondary lymphoid organs and blood concurrent with lack of replacement either through homeostatic proliferation of memory T cells or through generation of new T cells from the thymus results in a sustained state of immunosuppression. This is exemplified by our demonstrated use of VSV vectors that failed to induce memory T-cell reactivation in glioma-bearing mice (Fig. 5). This finding suggests both homeostatic proliferation and pre-existing memory responses are likely diminished in patients with GBM or patients with other neurological diseases.

T-cell sequestration in the bone marrow has a complex mechanism

We reported T-cell sequestration within the bone marrow using the GL261-model of GBM (Supplementary Fig. 3, similar to Chongsathidkiet *et al.*, 2018). This population mainly consists of naïve and central memory CD4 T cells (Supplementary Fig. 3). Using parabiosis, we further demonstrated that while the sequestration of bone marrow T cells occurs only in the glioma-bearing parabiont, a change in phenotype of bone marrow resident T cells was evident in both parabionts compared to naïve-naïve parabionts (Fig. 5). This demonstrated that soluble factors are affecting the phenotype of T cells in the bone marrow niche. Meanwhile, overall T-cell sequestration is potentially due to neuronal connections between the brain and bone marrow and not due to circulating factors in glioma-bearing mice.

A modest increase in bone marrow T cells cannot elucidate severe defects in all immune organs

It has been put forward that T-cell sequestration in the bone marrow is a component of experimental GBM-induced immunosuppression (Chongsathidkiet *et al.*, 2018). We, too, observe this in our studies (Supplementary Fig. 3). However, mathematically we contend this sequestration does not account for the magnitude of the multifaceted immune suppression we observe. We calculated mean thymic cellularity, spleen cellularity, numbers of CD4 T cells per 100 µl of blood, and numbers of accumulated T cells in the bone marrow of naïve and GL261-bearing mice to obtain values that represent average cell loss/gain within our experiments. Comparing naïve to glioma-bearing mice, 57 million cells from the thymus, and 18 million cells from the spleen were lost. In spleen alone, CD4 T-cells declined on average by 3.8 million cells. Similarly, blood CD4 T-cell compartment was reduced by about 7900 cells per 100 µl volume of blood. Assuming a mouse has about –1.5ml of blood by volume, we can estimate an approximate loss of 80 000–83 000 CD4

T cells from blood alone. In contrast to these significant losses, the bone marrow T-cell compartment only expanded on average by 286 000 cells. The gain in bone marrow resident CD4 T cells was equivalent to ~140 000 cells. We realize that accounting for changes within two femurs does not fully recapitulate numbers in the entire mouse bone marrow. Nevertheless, loss of 57 million thymocytes, 3.8 million splenic CD4 T cells, and 83 000 blood CD4 T cells cannot be explained through a modest increase of 140 000 CD4 T cells in the bone marrow. Additionally, all T cells, including naïve and memory, are lost at equal levels from both spleen and blood, yet we only observe marked enrichment in bone marrow resident naïve CD4 T cells. We did not observe evidence of premature exit of thymocytes from the thymus, nor did we observe accumulation of T cells with a double-positive phenotype in blood or bone marrow. T-cell accumulation in the bone marrow does not explain lack of responses by pre-existing memory T cells either. We therefore contend, through completion of the above analysis, that bone marrow sequestration of resident T cells is not the sole mechanism of neurological injury-induced immunosuppression.

Systemic immunosuppression caused by brain cancer may be restored through targeting circulation

This study creates a path forward to reverse systemic immunosuppression through targeting of serum-derived factors. Interestingly, adrenalectomized mice implanted with GL261 gliomas did not have thymic involution, spleen atrophy, evident loss of T cells, downregulation of MHCII expression, or sequestration of T cells within the bone marrow. However, glioma-bearing adrenalectomized mice did harbour potent immunosuppressive factor(s) in serum, and this alone translated into similar anti-tumour responses and survival kinetics compared to wild-type mice (Fig. 8 and Supplementary Table 1). Therefore, we hypothesize that reversing immunosuppression mediated through serum-derived factors should be the first step in restoring immunity in patients with GBM. In the absence of developing strategies to reverse serum-derived immunosuppression, attempts to target other facets of immunosuppression may fail. Hence, reversal of immunosuppression in serum could be the first step in reversing systemic immunosuppression as it will likely lead to enhanced thymic development. This in turn will enhance T-cell numbers in the periphery. In parallel, removing the anti-proliferative factor from serum will potentiate homeostatic proliferation and T-cell activation while boosting naïve and memory T-cell responses. Conceptually, this strategy would improve endogenous anti-tumour responses and immunotherapy outcomes. Identifying serum-derived non-steroid immunosuppressive factor(s) is therefore crucial in understanding and reversing immunosuppression during neurological insults to improve current and future therapies for patients with GBM, and the large cohort of patients with other neurological diseases.

Competing interests

The authors report no competing interests.

Supplementary material

Supplementary material is available at *Brain* online.

References

Andaloussi AE, Han Y, Lesniak MS. Progression of intracranial glioma disrupts thymic homeostasis and induces T-cell apoptosis in vivo. Cancer Immunol Immunother 2008; 57: 1807–16.

Antonica A, Magni F, Mearini L, Paolocci N. Vegal control of lymphocyte release from rat thymus. J Auton Nervous Syst 1994; 48: 187–97.

Ayasoufi K, Fan R, Valujskikh A. Depletion-resistant CD4 T cells enhance thymopoiesis during lymphopenia. Am J Transplant 2017; 17: 2008–19.

Ayasoufi K, Pfaller CK, Khadka RH, Jin F, Johnson AJ. Brain-Thymus communication is a novel immunosuppressive feature of neurological insults. J Immunol 2019; 202(1 Supplement):183.19.

Baral P, Umans BD, Li L, Wallrapp A, Bist M, Kirschbaum T, et al. Nociceptor sensory neurons suppress neutrophil and gammadelta T cell responses in bacterial lung infections and lethal pneumonia. Nat Med 2018; 24: 417–26.

Bell MP, Renner DN, Johnson AJ, Pavelko KD. An elite controller of picornavirus infection targets an epitope that is resistant to immune escape. PLoS One 2014; 9: e94332.

Chen AL, Sun X, Wang W, Liu JF, Zeng X, Qiu JF, et al. Activation of the hypothalamic-pituitary-adrenal (HPA) axis contributes to the immunosuppression of mice infected with Angiostrongylus cantonensis. J Neuroinflammation 2016; 13: 266.

Chongsathidkiet P, Jackson C, Koyama S, Loebel F, Cui X, Farber SH, et al. Sequestration of T cells in bone marrow in the setting of glioblastoma and other intracranial tumors. Nat Med 2018; 24: 1459–68.

Cordero FJ, Huang Z, Grenier C, He X, Hu G, McLendon RE, et al. Histone H3.3K27M represses p16 to accelerate gliomagenesis in a murine model of DIPG. Mol Cancer Res 2017; 15: 1243–54.

Cumba Garcia LM, Huseby Kelcher AM, Malo CS, Johnson AJ. Superior isolation of antigen-specific brain infiltrating T cells using manual homogenization technique. J Immunol Methods 2016; 439: 23–8.

Dix A, Brooks W, Roszman T, Morford L. Immune defects observed in patients with primary malignant brain tumors. J Neuroimmunol 1999; 100: 17.

Eyo UB, Peng J, Swiatkowski P, Mukherjee A, Bispo A, Wu LJ. Neuronal hyperactivity recruits microglial processes via neuronal NMDA receptors and microglial P2Y12 receptors after status epilepticus. J Neurosci 2014; 34: 10528–40.

Fecci PE, Mitchell DA, Whitesides JF, Xie W, Friedman AH, Archer GE, et al. Increased regulatory T-cell fraction amidst a diminished CD4 compartment explains cellular immune defects in patients with malignant glioma. Cancer Res 2006; 66: 3294–302.

Ferrando-Martínez S, Franco JM, Hernandez A, Ordoñez A, Gutierrez E, Abad A, et al. Thymopoiesis in elderly human is associated with systemic inflammatory status. Age 2009; 31: 87–97.

Ferretti MT, Merlini M, Spani C, Gericke C, Schweizer N, Enzmann G, et al. T-cell brain infiltration and immature antigen-presenting cells in transgenic models of Alzheimer's disease-like cerebral amyloidosis. Brain Behav Immun 2016; 54: 211–25.

Garcia-Ojeda ME, Klein Wolterink RG, Lemaitre F, Richard-Le Goff O, Hasan M, Hendriks RW, et al. GATA-3 promotes T-cell specification by repressing B-cell potential in pro-T cells in mice. Blood 2013; 121: 1749–59.

Godfraind C, Coutelier JP. Morphological analysis of mouse hepatitis virus A59-induced pathology with regard to viral receptor expression. Histol Histopathol 1998; 13: 181–99.

Godfraind C, Holmes KV, Coutelier JP. Thymus involution induced by mouse hepatitis virus A59 in BALB/c mice. J Virol 1995; 69: 6541–7.

Grossman SA, Ye X, Lesser G, Sloan A, Carraway H, Desideri S, et al. Immunosuppression in patients with high-grade gliomas treated with radiation and temozolomide. Clin Cancer Res 2011; 17: 5473–80.

Gruver AL, Sempowski GD. Cytokines, leptin, and stress-induced thymic atrophy. J Leukoc Biol 2008; 84: 915–23.

Gurkan S, Luan Y, Dhillon N, Allam SR, Montague T, Bromberg JS, et al. Immune reconstitution following rabbit antithymocyte globulin. Am J Transplant 2010; 10: 2132–41.

Gustafson MP, Lin Y, New KC, Bulur PA, O'Neill BP, Gastineau DA, et al. Systemic immune suppression in glioblastoma: the interplay between CD14 + HLA-DRlo/neg monocytes, tumor factors, and dexamethasone. Neuro Oncol 2010; 12: 631–44.

Haile Y, Carmine-Simmen K, Olechowski C, Kerr B, Bleackley RC, Giuliani F. Granzyme B-inhibitor serpina3n induces neuroprotection in vitro and in vivo. J Neuroinflammation 2015; 12: 157.

Hazeldine J, Lord JM, Belli A. Traumatic brain injury and peripheral immune suppression: primer and prospectus. Front Neurol 2015; 6:

Hsu I, Parkinson LG, Shen Y, Toro A, Brown T, Zhao H, et al. Serpina3n accelerates tissue repair in a diabetic mouse model of delayed wound healing. Cell Death Dis 2014; 5: e1458.

Huggins MA, Johnson HL, Jin F, Songo AN, Hanson LM, LaFrance SJ, et al. Perforin expression by CD8 T cells is sufficient to cause fatal brain edema during experimental cerebral malaria. Infect Immun 2017; 85: e00985–16.

Huseby Kelcher AM, Atanga PA, Gamez JD, Cumba Garcia LM, Teclaw SJ, Pavelko KD, et al. Brain atrophy in picornavirus-infected FVB mice is dependent on the H-2Db class I molecule. FASEB J 2017; 31: 2267–75.

Jamieson B, Douek D, Killian S, Hultin L, Scripture-Adams D, Giorgi J, et al. Generation of functional thymocytes in the human adult. Immunity 1999; 10: 7.

Johnson AJ, Mendez-Fernandez Y, Moyer AM, Sloma CR, Pirko I, Block MS, et al. Antigen-Specific CD8 + T cells mediate a peptide-induced fatal syndrome. J Immunol 2005; 174: 6854–62.

Kamran P, Sereti K-I, Zhao P, Ali SR, Weissman IL, Ardehali R. Parabiosis in mice: a detailed protocol. J Vis Exp 2013; 80: 50556.

Kendall M, Al-Shawaf A. Innervation of the rat thymus gland. Brain Behav Immun 1991; 5: 20.

Kipnis J, Filiano AJ. Neuroimmunology in 2017: the central nervous system: privileged by immune connections. Nat Rev Immunol 2018; 18: 83–4.

Laurent C, Dorothee G, Hunot S, Martin E, Monnet Y, Duchamp M, et al. Hippocampal T cell infiltration promotes neuroinflammation and cognitive decline in a mouse model of tauopathy. Brain 2017; 140: 184–200.

Lewicki H, Tishon A, Homann D, Mazarguil H, Laval F, Asensio VC, et al. T cells infiltrate the brain in murine and human transmissible spongiform encephalopathies. J Virol 2003; 77: 3799–808.

Liu Q, Jin WN, Liu Y, Shi K, Sun H, Zhang F, et al. Brain ischemia suppresses immunity in the periphery and brain via different neurogenic innervations. Immunity 2017; 46: 474–87.

Mackall CL, Fry TJ, Bare C, Morgan P, Galbraith A, Gress RE. IL-7 increases both thymic-dependent and thymic-independent T-cell regeneration after bone marrow transplantation. Blood 2001; 97: 8.

Malo CS, Huggins MA, Goddery EN, Tolcher HMA, Renner DN, Jin F, et al. Non-equivalent antigen presenting capabilities of dendritic cells and macrophages in generating brain-infiltrating CD8 (+) T cell responses. Nat Commun 2018a; 9: 633.

Malo CS, Khadka RH, Ayasoufi K, Jin F, AbouChehade JE, Hansen MJ, et al. Immunomodulation mediated by anti-angiogenic therapy improves CD8 T cell immunity against experimental glioma. Front Oncol 2018b; 8: 320.

Maryanovich M, Zahalka AH, Pierce H, Pinho S, Nakahara F, Asada N, et al. Adrenergic nerve degeneration in bone marrow drives aging of the hematopoietic stem cell niche. Nat Med 2018; 24: 782–91.

McDole J, Johnson AJ, Pirko I. The role of CD8 + T-cells in lesion formation and axonal dysfunction in multiple sclerosis. Neurol Res 2006; 28: 256–61.

Meisel C, Schwab JM, Prass K, Meisel A, Dirnagl U. Central nervous system injury-induced immune deficiency syndrome. Nat Rev Neurosci 2005; 6: 775–86.

Mignini F, Streccioni V, Amenta F. Autonomic innervation of immune organs and neuroimmune modulation. Auton Autacoid Pharmacol 2003; 23: 25.

Ostrom QT, Gittleman H, Fulop J, Liu M, Blanda R, Kromer C, et al. CBTRUS statistical report: primary brain and central nervous system tumors diagnosed in the United States in 2008-2012. Neuro Oncol 2015; 17 (Suppl 4): iv1–iv62.

Pavelko KD, Girtman MA, Mitsunaga Y, Mendez-Fernandez YV, Bell MP, Hansen MJ, et al. Theiler's murine encephalomyelitis virus as a vaccine candidate for immunotherapy. PLoS One 2011; 6: e20217.

Pfaller CK, Donohue RC, Nersisyan S, Brodsky L, Cattaneo R. Extensive editing of cellular and viral double-stranded RNA structures accounts for innate immunity suppression and the proviral activity of ADAR1p150. PLoS Biol 2018; 16: e2006577.

Pinho-Ribeiro FA, Baddal B, Haarsma R, O'Seaghdha M, Yang NJ, Blake KJ, et al. Blocking neuronal signaling to immune cells treats streptococcal invasive infection. Cell 2018; 173: 1083–97.e22.

Racine R. Modification of Seizure activity by electrical stimulation: II. Motor Seizure. Electroencephalogr Clin Neurophysiol 1972; 32: 14.

Ransehoff R. Immune-cell crosstalk in multiple sclerosis. Nature 2018; 563: 2.

Ritzel RM, Doran SJ, Barrett JP, Henry RJ, Ma EL, Faden AI, et al. Chronic alterations in systemic immune function after traumatic brain injury. J Neurotrauma 2018; 35: 1419–36.

Rosado-Sanchez I, Herrero-Fernandez I, Genebat M, Ruiz-Mateos E, Leal M, Pacheco YM. Thymic function impacts the peripheral CD4/CD8 ratio of HIV-infected subjects. Clin Infect Dis 2017; 64: 152–8.

Rothenberg EV. Programming for T-lymphocyte fates: modularity and mechanisms. Genes Dev 2019; 33: 1117–35.

Roux E, Dumont-Girard F, Starobinski M, Siegrist C, Helg C, Chapuis B, et al. Recovery of immune reactivity after T-cell–depleted bone marrow transplantation depends on thymic activity. Blood 2000; 96: 6.

Scripture-Adams DD, Damle SS, Li L, Elihu KJ, Qin S, Arias AM, et al. GATA-3 dose-dependent checkpoints in early T cell commitment. J Immunol 2014; 193: 3470–91.

Sergi D, Campbell FM, Grant C, Morris AC, Bachmair EM, Koch C, et al. SerpinA3N is a novel hypothalamic gene upregulated by a high-fat diet and leptin in mice. Genes Nutr 2018; 13: 28.

Stanley D, Mason LJ, Mackin KE, Srikhanta YN, Lyras D, Prakash MD, et al. Translocation and dissemination of commensal bacteria in post-stroke infection. Nat Med 2016; 22: 1277–84.

Takamiya A, Takeda M, Yoshida A, Kiyama H. Inflammaton induces serine protease inhibitor 3 expression in the rat pineal gland. Neuroscience 2002; 113: 8.

Talbot S, Abdulnour RE, Burkett PR, Lee S, Cronin SJ, Pascal MA, et al. Silencing nociceptor neurons reduces allergic airway inflammation. Neuron 2015; 87: 341–54.

Tibbetts TA, DeMayo F, Rich S, Conneely OM, O'Malley BW. Progesterone receptors in the thymus are required for thymic involution during pregnancy and for normal fertility. Proc Natl Acad Sci USA 1999; 96: 12021–6.

Tsunoda I, Sato F, Omura S, Fujita M, Sakiyama N, Park AM. Three immune-mediated disease models induced by Theiler's virus: multiple sclerosis, seizures and myocarditis. Clin Exp Neuroimmunol 2016; 7: 330–45.

van den Broek T, Delemarre EM, Janssen WJ, Nievelstein RA, Broen JC, Tesselaar K, et al. Neonatal thymectomy reveals differentiation and plasticity within human naive T cells. J Clin Invest 2016; 126: 1126–36.

Vega EA, Graner MW, Sampson JH. Combating immunosuppression in glioma. Future Oncol 2008; 4: 433–42.

Verinaud L, Da Cruz-Hofling MA, Sakurada JK, Rangel HA, Vassallo J, Wakelin D, et al. Immunodepression induced by Trypanosoma cruzi and mouse hepatitis virus type 3 is associated with thymus apoptosis. Clin Diagn Lab Immunol 1998; 5: 186–91.

Vicuna L, Strochlic DE, Latremoliere A, Bali KK, Simonetti M, Husainie D, et al. The serine protease inhibitor SerpinA3N attenuates neuropathic pain by inhibiting T cell-derived leukocyte elastase. Nat Med 2015; 21: 518–23.

Voisin T, Bouvier A, Chiu IM. Neuro-immune interactions in allergic diseases: novel targets for therapeutics. Int Immunol 2017; 29: 247–61.

Weinberg K, Blazar B, Wagner J, Agura E, Hill B, Smogorzewska M, et al. Factors affecting thymic function after allogeneic hematopoietic stem cell transplantation. Blood 2001; 97: 10.

Willenbring RC, Jin F, Hinton DJ, Hansen M, Choi D-S, Pavelko KD, et al. Modulatory effects of perforin gene dosage on pathogen-associated blood-brain barrier (BBB) disruption. J Neuroinflammation 2016; 13:222.

Williams KM, Hakim FT, Gress RE. T cell immune reconstitution following lymphodepletion. Semin Immunol 2007; 19: 318–30.

Wong C, Jenne CN, Lee WY, Leger C, Kubes P. Functional innervation of hepatic iNKT cells is immunosuppressive following stroke. Science 2011; 334: 6.

Wongthida P, Diaz RM, Pulido C, Rommelfanger D, Galivo F, Kaluza K, et al. Activating systemic T-cell immunity against self tumor antigens to support oncolytic virotherapy with vesicular stomatitis virus. Hum Gene Ther 2011; 22: 1343–53.

Youm YH, Horvath TL, Mangelsdorf DJ, Kliewer SA, Dixit VD. Prolongevity hormone FGF21 protects against immune senescence by delaying age-related thymic involution. Proc Natl Acad Sci USA 2016; 113: 1026–31.

Zhang L, Lewin SR, Markowitz M, Lin H-H, Skulsky E, Karanicolas R, et al. Measuring recent thymic emigrants in blood of normal and HIV-1–infected individuals before and after effective therapy. J Exp Med 1999; 190: 8.

Zhou Y, Song WM, Andhey PS, Swain A, Levy T, Miller KR, et al. Human and mouse single-nucleus transcriptomics reveal TREM2-dependent and TREM2-independent cellular responses in Alzheimer's disease. Nat Med 2020; 26: 131–42.

Zook EC, Krishack PA, Zhang S, Zeleznik-Le NJ, Firulli AB, Witte PL, et al. Overexpression of Foxn1 attenuates age-associated thymic involution and prevents the expansion of peripheral CD4 memory T cells. Blood 2011; 118: 5723–31.